

# Pulling Target to Source: A New Perspective on Domain Adaptive Semantic Segmentation

Haochen Wang<sup>1,2</sup> · Yujun Shen<sup>4</sup> · Jingjing Fei<sup>5</sup> · Wei Li<sup>5</sup> · Liwei Wu<sup>5</sup>  
Yuxi Wang<sup>3\*</sup> · Zhaoxiang Zhang<sup>1,2,3\*</sup>

Received: date / Accepted: date

**Abstract** Domain-adaptive semantic segmentation aims to transfer knowledge from a labeled source domain to an unlabeled target domain. However, existing methods primarily focus on directly learning categorically discriminative target features for segmenting target images, which is challenging in the absence of target labels. This work provides a new perspective. We observe that the features learned with source data manage to keep categorically discriminative during training, thereby enabling us to implicitly learn adequate target representations by simply *pulling target features close to source features for each category*. To this end, we propose T2S-DA, which encourages the model to learn similar cross-domain features. Also, considering the pixel categories are heavily imbalanced for segmentation datasets, we come up with a dynamic re-weighting strategy to help the model concentrate on those underperforming classes. Extensive experiments confirm that T2S-DA learns a more discriminative and generalizable representation, significantly surpassing the state-of-the-art. We further show that T2S-DA is quite qualified for the domain generalization task, verifying its domain-invariant property.

**Keywords** Domain Adaptation · Semantic Segmentation

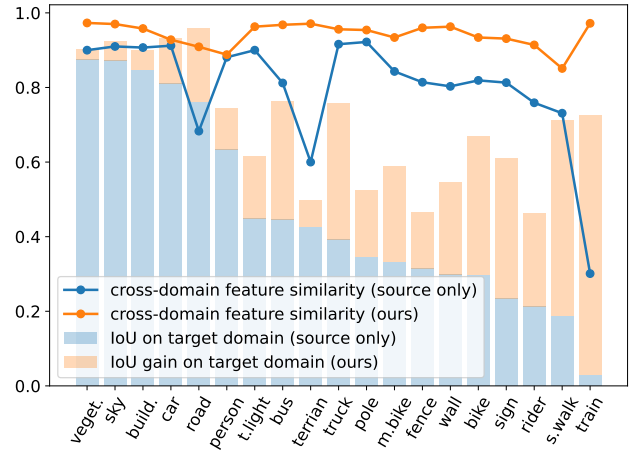


**Fig. 1** Category-wise cross-domain feature similarity as well as the evaluation results on the target domain. When directly testing the model trained with source data (i.e., “source only”) on the target data, the categories, where source and target features are largely dissimilar to each other, suffer from low IoU.

## 1 Introduction

The success of semantic segmentation largely relies on big data (Long et al., 2015a; Ronneberger et al., 2015; Zhao et al., 2017), however, collecting a sufficient number of annotated images could be labor-intensive in practice (Cordts et al., 2016; Zhou et al., 2017). Recent studies (Zhang et al., 2019; Kang et al., 2020; Araslanov and Roth, 2021; Hoyer et al., 2022a) yield an alternative solution by introducing synthetic datasets (Richter et al., 2016; Ros et al., 2016), where the labels can be obtained with minor effort. However, the models learned on these datasets are found hard to generalize to real-world scenarios. To address this challenge, unsupervised domain adaptation (UDA) (Zou et al., 2018; Vu et al., 2019; Lian et al., 2019; Chen et al., 2022a) is proposed to transfer knowledge from the labeled source

<sup>1</sup> New Laboratory of Pattern Recognition, State Key Laboratory of Multimodal Artificial Intelligence Systems, Institute of Automation, Chinese Academy of Sciences, Beijing, China.

<sup>2</sup> University of Chinese Academy of Sciences, Beijing, China.

<sup>3</sup> Centre for Artificial Intelligence and Robotics, Hong Kong Institute of Science & Innovation, Chinese Academy of Sciences, Hong Kong, China.

<sup>4</sup> Chinese University of Hong Kong, Hong Kong, China.

<sup>5</sup> SenseTime Research, Beijing, China.

\* Yuxi Wang and Zhaoxiang Zhang are the corresponding authors.

E-mail: {wanghaochen2022, zhaoxiang.zhang}@ia.ac.cn, and yuxi-wang93@gmail.com.

domain (*e.g.*, synthetic) to an unlabeled target domain (*e.g.*, real). Under this setting, the crux becomes how to make full use of source labels to learn discriminative representations for segmenting target samples.

To address this issue, typical solutions fall into two categories, *i.e.*, adversarial training, and self-training. The former tries to align the feature distribution of different domains to an *intermediate common space* (Goodfellow et al., 2014; Nowozin et al., 2016; Tsai et al., 2018; Luo et al., 2019; Chen et al., 2019b; Tsai et al., 2019; Pan et al., 2020; Wang et al., 2020b; Luo et al., 2021; Ganin et al., 2016; Long et al., 2018). Although these approaches converge the two domains globally, it is hard to ensure that target features from different categories are well-separated (Xie et al., 2023; Du et al., 2022b). The latter aims to build a capable *target* feature space by selecting confident target predictions as pseudo-ground truths (Tranheden et al., 2021; Zou et al., 2019; Zhang et al., 2019; Li et al., 2022; Zheng and Yang, 2021; Araslanov and Roth, 2021; Shin et al., 2020; Du et al., 2022b; Yang and Soatto, 2020; Wang et al., 2023e; Chen et al., 2022b). These approaches *directly* supervise the model with target pseudo-labels. However, the segmentation model usually tends to be biased to the source domain, resulting in error-prone target pseudo-labels (Li et al., 2022).

We first explore the underlying causes of the performance drop and the consequences of the distribution shift when applying the model trained on source data to target data. As blue bars in Fig. 1 suggest, *not all* categories suffer in this domain shift. Specifically, the performances of “vegetation”, “sky”, and “building” manage to remain satisfactory under the domain gap. However, the performance of “train” deteriorates severely under this setting. The main differences between these two types of categories are *feature dissimilarities*. Concretely, features of those underperforming classes are *dissimilar* across domains, *i.e.*, with *small* similarity.

Based on this evidence, we aim to design a framework that can extract *similar* cross-domain features regarding each category. Intuitively, source features are *always* categorically discriminative during training thanks to sufficient source labels. Therefore, as illustrated in Fig. 2, we argue that (1) discriminative source features plus (2) urging target features to be similar to the source feature for each category, implicitly brings the categorical discriminativeness of target features. To this end, we propose T2S-DA, regarding source features as *anchors* and explicitly pulling target features *close* to source ones. However, due to the lack of target labels, it is hard to conduct feature pairs that *exactly* belong to the same class.

To address this issue, we employ an image translation engine to produce pseudo-images by transferring source data to the target style. These pseudo-images are then served as queries and can be easily matched with their positive keys (*i.e.*, source features from the same category) *precisely* since they naturally have annotations. Additionally, considering

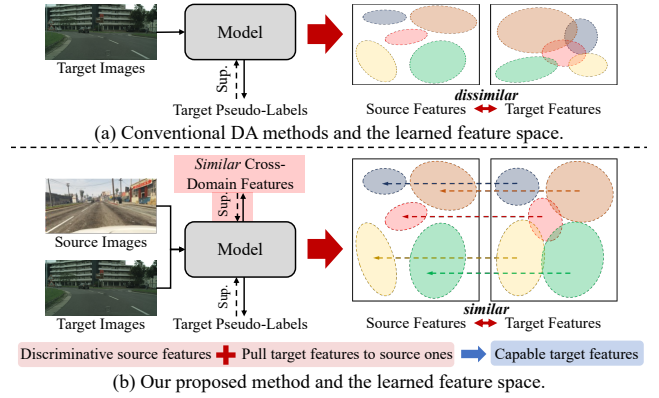


**Fig. 2 Concept comparison** between (a) conventional methods and (b) our T2S-DA. To obtain discriminative features from target images, existing approaches *directly* supervise the model with target pseudo-labels regardless of the similarity between cross-domain features. Differently, T2S-DA addresses this issue from a new perspective, where we argue that “discriminative source features” plus “making target features close to source features” *implicitly* brings capable target features.

the pixel categories are heavily imbalanced for segmentation datasets, we put forward a dynamic re-weighting strategy, forcing the model to put more effort into those underperforming classes. Through this way, our approach is able to learn similar representations across domains and hence achieves substantial improvements on the target domain. From Fig. 1, we can tell that *the improved similarity indeed contributes to better performances*, especially for class “train”.

We evaluate the proposed T2S-DA on two UDA benchmarks, *i.e.*, GTA5 (Richter et al., 2016) → Cityscapes (Cordts et al., 2016) and Synthia (Ros et al., 2016) → Cityscapes (Cordts et al., 2016), where we consistently surpass state-of-the-art alternatives. For instance, T2S-DA achieves 75.1% mIoU on GTA5 → Cityscapes benchmark, outperforming HRDA (Hoyer et al., 2022b) by +1.3%. Moreover, we find T2S-DA is also applicable to the domain generalization task, where the training phase cannot access the target samples at all. Under this setting, when training the model on GTA5 and Synthia and testing on Cityscapes, we improve the baseline by +2.5% and +2.1%, respectively.

## 2 Related Work

### 2.1 Domain Adaptive Semantic Segmentation

Domain adaptive semantic segmentation aims at learning a generalized segmentation model that can adapt from a labeled (synthetic) source domain to an unlabeled (real-world) target domain. To overcome the domain gap, most previous methods align distributions of source and target domains to an *intermediate common space* at the image level (Hoffman et al., 2018; Murez et al., 2018; Sankaranarayanan et al., 2018; Li et al., 2019c), feature level (Hoffman et al., 2016; Hong et al., 2018; Saito et al., 2018; Chang et al., 2019;

Chen et al., 2019a), and output level (Tsai et al., 2018; Luo et al., 2019) by introducing extra objectives or techniques, e.g., optimizing some custom distance (Long et al., 2015b; Lee et al., 2019), applying computationally adversarial training (Goodfellow et al., 2014; Nowozin et al., 2016; Tsai et al., 2018; Luo et al., 2019; Chen et al., 2019b; Tsai et al., 2019), offline pseudo-labeling (Zou et al., 2018; Li et al., 2019c; Zou et al., 2019), and image translation models (Hoffman et al., 2018; Li et al., 2019c). Different from these methods, as illustrated in Fig. 2b, based on the observation that source features are always capable during training, we *pull target features close to source features for each category*. Through this way, T2S-DA manages to learn similar cross-domain features for each category. Shown in Fig. 1, the improved cross-domain feature similarity indeed boosts the segmentation results. One may be concerned that making the source close to the target seems to be a reasonable alternative. We compare this strategy, i.e., “source  $\rightarrow$  target”, to our T2S-DA in Sec. 4.3, where we empirically find that this explicit alignment works *only when pulling target to source*.

## 2.2 Domain Generalized Semantic Segmentation

Domain generalized semantic segmentation is a more challenging task compared to domain adaptation. It assumes target data is inaccessible during training, focusing on generalizing well on *unseen* target domains. To extract domain-invariant feature representations, plenty of approaches have been proposed such as meta-learning (Li et al., 2018a; Balaji et al., 2018; Li et al., 2019a,b), adversarial training (Li et al., 2018b,c; Rahman et al., 2020), metric-learning (Motiian et al., 2017; Dou et al., 2019), and feature normalization (Pan et al., 2018; Huang et al., 2019; Choi et al., 2021). Few attempts have been made in domain generalization based on cross-domain alignment. T2S-DA is proved to be efficient for both settings, verifying that similar cross-domain features do contribute to better segmentation results.

## 2.3 Contrastive Learning in Semantic Segmentation

Recently, contrastive learning has been verified to be a successful framework for unsupervised or self-supervised representation learning in computer vision (He et al., 2020; Grill et al., 2020; Li et al., 2021; Chen et al., 2020; Chen and He, 2021; Caron et al., 2021; Wang et al., 2023a,b,c, 2024), and has been explored in fully-supervised (Wang et al., 2021a; Hu et al., 2021), semi-supervised (Wang et al., 2022; Liu et al., 2022; Wang et al., 2023d), and weakly-supervised (Du et al., 2022a) semantic segmentation. Only a few studies introduce contrastive learning in domain adaptive semantic segmentation. Let us consider leveraging contrastive learning to minimize the domain gap. It becomes crucial that

**Table 1** Comparison among domain adaptive semantic segmentation methods using contrastive learning. Our T2S-DA makes positive pairs are (1) matched precisely and (2) across domains.

Method	Queries	Positive Keys	Positive pairs are	
			matched precisely	across domains
(Kang et al., 2020)	source	target	✗	✓
(Huang et al., 2022)	target	source + target	✗	✗
(Zhou et al., 2022)	target	target	✓	✗
(Huang et al., 2021b)	target	target	✓	✗
T2S-DA (ours)	p. target	source	✓	✓

positive pairs should be (1) matched precisely at the category level and (2) across domains, regardless of the level where the contrast is conducted. In the literature, contrast is conducted at pixel (Kang et al., 2020), category (Huang et al., 2022), region (Zhou et al., 2022), and history (Huang et al., 2021b) levels, respectively. T2S-DA is the only one that both satisfies (1) and (2). Specifically, it conducts contrast at the category level *across domains*. By employing an image translation engine, T2S-DA is a more efficient framework since it *ensures cross-domain features are matched correctly* when conducting positive pairs. We summarize these two properties in Tab. 1. Interestingly, consistent improvements are observed by simply minimizing MSE between  $\ell_2$  normalized positive pairs, verifying that contrastive learning is *not* the only way of pulling target to source.

## 2.4 Discrepancy-based Domain Adaptation

Most previous discrepancy-based methods align source and target domains via adversarial learning (Goodfellow et al., 2014). Specifically, (Saito et al., 2018) maximizes and minimizes the discrepancy on target by introducing an adversarial objective in the second and third stages, respectively. (Ganin et al., 2016) proposed domain-adversarial neural networks motivated by the theoretical analysis by (Ben-David et al., 2006). (Tzeng et al., 2017) combined discriminative modeling, untied weight sharing, and a GAN loss. (Bousmalis et al., 2017) and (Hoffman et al., 2018) further leveraged image translation models to minimize the domain discrepancy by cheating the discriminator. The main difference between our T2S-DA and those GAN-based methods is that T2S-DA regards the labeled source domain as *anchors* and *explicitly aligns the joint feature distribution to the source feature space*, while those methods implicitly align cross-domain features to an *intermediate common space*. The advantage of pulling target to source compared with aligning to a common space is that our T2S-DA manages to keep the performance on the *source* domain (Tab. 17), while GAN-based methods are expected to perform worse than the source-only baseline on the source domain. This indicates that T2S-DA learns more robust features and has better generalization abilities, since T2S-DA improves the performance on *both*

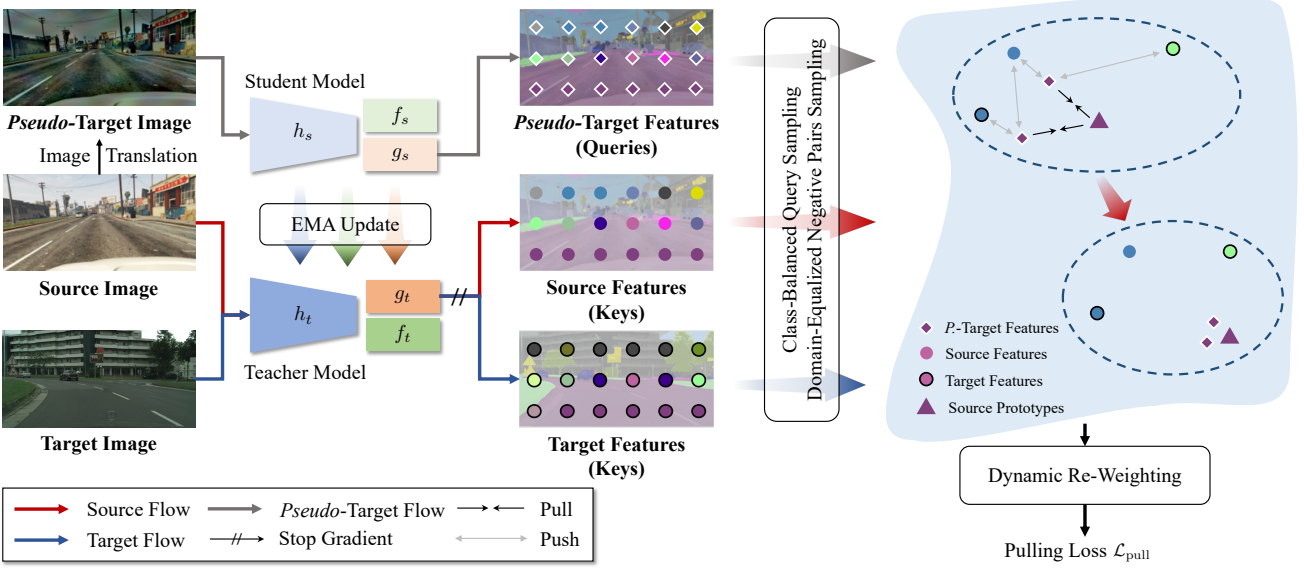


**Fig. 3 Illustration of contrastive pairs.** We regard features from *pseudo-targets* and *source prototypes* of the same category as the positive pairs defined in Eq. (10). Negative keys include 1) source features from a different category (as in Eq. (12)), and 2) unreliable target features from a different category (as in Eq. (13)). In this way, this model is encouraged to *learn similar features between the source and target domains from any category*. The improved similarity indeed boosts segmentation results (see Fig. 1).

domains. Another line of work directly minimizes the distance between the feature distributions of different domains. Specifically, DAN (Long et al., 2015b) proposes an MK-MMD (Gretton et al., 2012)-based multi-layer adaptation regularizer, which is activated in the last three linear layers of a CNN. RTN (Long et al., 2016), on the basis of DAN, assumes that source and target classifiers differ by a residual function, and applies extra classifier adaption via a newly proposed residual transfer module. Deep CORAL (Sun and Saenko, 2016) extends CORAL (Sun et al., 2016), which aligns the second-order statistics of the source and target distributions, to deep models through an auxiliary loss function for cross-domain outputs. Compared with these distance-based methods (Sun and Saenko, 2016; Long et al., 2015b, 2016), this work does not aim to explore a specific distance. We demonstrate that as long as regarding source features as anchors and pulling target features close to source ones for each category, a simple MSE manages to be effective.

### 3 Method

#### 3.1 Overview

Unsupervised domain adaptive semantic segmentation aims at applying a model learned from the labeled source dataset  $\mathcal{D}_s = \{(\mathbf{x}_i^s, \mathbf{y}_i^s)\}_{i=1}^{n_s}$  to the unlabeled target dataset  $\mathcal{D}_t = \{\mathbf{x}_i^t\}_{i=1}^{n_t}$ , where  $n_s$  and  $n_t$  are the numbers of images of source and target domains, respectively.  $\mathbf{x}_i^s \in \mathbb{R}^{H \times W \times 3}$  and  $\mathbf{x}_i^t \in \mathbb{R}^{H \times W \times 3}$  are RGB images, while  $\mathbf{y}_i^s \in \mathbb{R}^{H \times W \times C}$  is the one-hot semantic map associated with  $\mathbf{x}_i^s$ . Source and target datasets share the same label space with  $C$  categories.

Following previous methods (Hoyer et al., 2022a; Zhang et al., 2021; Li et al., 2022; Du et al., 2022b; Wang et al., 2023c), we adopt self-training as the baseline, where source data are used under a supervised manner and the unsupervised loss is computed based on target images and their pseudo-labels generated by a momentum teacher. Concretely, our proposed T2S-DA follows the Mean Teacher (Tarvainen and Valpola, 2017) framework that consists of a student and a teacher. Each model  $\psi$  reparameterized by  $\theta$  consists of an encoder  $h : \mathbb{R}^{H \times W \times 3} \rightarrow \mathbb{R}^{h \times w \times D}$  followed by a segmentor  $f : \mathbb{R}^{h \times w \times D} \rightarrow (0, 1)^{H \times W \times C}$  and a projector  $g : \mathbb{R}^{h \times w \times D} \rightarrow \mathbb{R}^{h \times w \times d}$ , where  $H$  and  $W$  indicate the height and width of the input image respectively.  $h$ ,  $w$  and  $D$  form the shape of the intermediate features, and  $d$  is the feature dimension of the projector. The teacher is momentum updated by the student, i.e.,  $\theta_t \leftarrow \eta \theta_t + (1 - \eta) \theta_s$ , where  $\eta$  is a momentum coefficient.  $\theta_s$  and  $\theta_t$  are parameters of the student  $\psi_s$  and the teacher  $\psi_t$ , respectively.

The overall objective is the sum of source supervised loss, target unsupervised loss, and pulling loss:  $\mathcal{L} = \mathcal{L}_{\text{source}} + \mathcal{L}_{\text{target}} + \lambda \mathcal{L}_{\text{pull}}$ . For source data, we naively train the student with categorical cross-entropy (CE)

$$\mathcal{L}_{\text{source}} = \sum_{i=1}^{n_s} \sum_{j=1}^{H \times W} \ell_{ce} [f_s(h_s(\mathbf{x}_i^s))](j), \mathbf{y}_i^s(j)], \quad (1)$$

where  $\ell_{ce}(\mathbf{p}, \mathbf{y}) = -\mathbf{y}^\top \log \mathbf{p}$ . For unlabeled target data, we adopt self-training, which minimizes the weighted cross-entropy loss between predictions and pseudo-labels  $\hat{\mathbf{y}}^t$  gen-

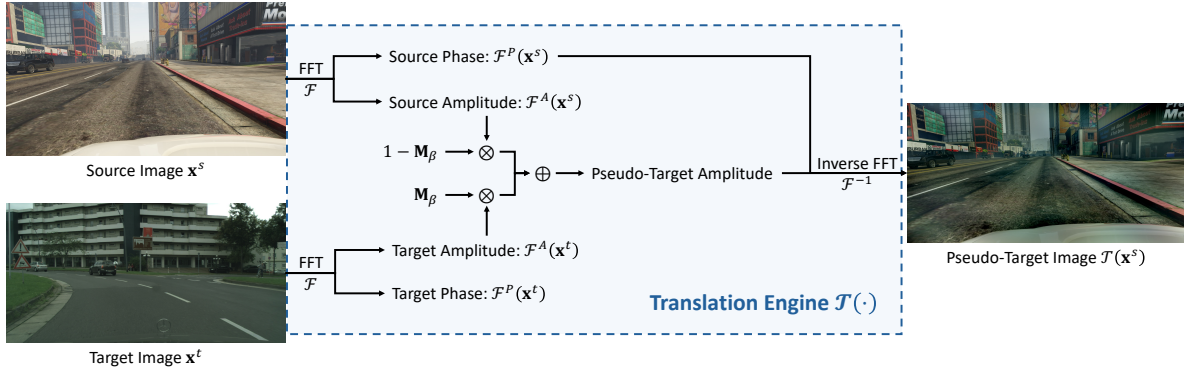


**Fig. 4** The pipeline of FDA (Yang and Soatto, 2020). Given a source image  $\mathbf{x}^s$  and a randomly sampled target image  $\mathbf{x}^t$ , FDA transfers the source image into target style, resulting in  $\mathcal{T}(\mathbf{x}^s)$ , by pasting the low-frequency part of the amplitude from the target sample to the source image.

erated by the teacher.

$$\mathcal{L}_{\text{target}} = \sum_{i=1}^{n_t} \sum_{j=1}^{H \times W} r_i^t \cdot \ell_{ce} [f_s(h_s(\mathbf{x}_i^t))(j), \hat{\mathbf{y}}_i^t(j)], \quad (2)$$

where  $\hat{\mathbf{y}}_i^t(j)$  is the one-hot pseudo-label generated by the teacher for  $i$ -th target image at position  $j$ . Moreover, following (Hoyer et al., 2022a) and (Tranheden et al., 2021), we use  $r_i^t$  the ratio of pixels whose softmax probability exceeds a threshold  $\delta_p$  to be the metric to measure the quality of pseudo-labels of the  $i$ -th target image:

$$r_i^t = \frac{1}{H \times W} \sum_{j=1}^{H \times W} \mathbb{1}[\max_c f_t \circ h_t(\mathbf{x}_i^t) > \delta_p], \quad (3)$$

where  $\mathbb{1}[\cdot]$  is the indicator function and  $\delta_p$  is set to 0.968 following (Tranheden et al., 2021).

As discussed in Sec. 1, we observe that the model trained with source data is able to build a capable source feature space, but when we apply it to target domain, the features run into undesirable chaos. *The performance drop is highly related to the cross-domain feature dissimilarity caused by the domain gap.* Intuitively, if we pull target features to source ones, it implicitly implies an adequate feature space for segmenting target samples. To this end, we aim to conduct *cross-domain positive pairs*, i.e.,  $(\mathbf{q}, \mathbf{k}^+)$ , from the *exactly* same category but different domains, and then maximize their agreement. We study two different objectives, including InfoNCE (Oord et al., 2018) and MSE. InfoNCE pulls together positive pairs  $(\mathbf{q}, \mathbf{k}^+)$  and pushes away negative pairs  $(\mathbf{q}, \mathbf{k}^-)$ .

$$\mathcal{L}_{\text{InfoNCE}}(\mathbf{q}, \mathbf{k}^+) = -\log \left[ \frac{e^{(\mathbf{q}^\top \mathbf{k}^+ / \tau)}}{e^{(\mathbf{q}^\top \mathbf{k}^+ / \tau)} + \sum_{\mathbf{k}^- \in \mathcal{K}_{\mathbf{q}}^-} e^{(\mathbf{q}^\top \mathbf{k}^- / \tau)}} \right], \quad (4)$$

where  $\mathbf{q}$ ,  $\mathbf{k}^+$  and  $\mathbf{k}^-$  are  $\ell_2$ -normalized features, which are outputs of the projector, indicating queries, positive keys,

and negative keys, respectively.  $\tau$  indicates the temperature.  $\mathcal{K}_{\mathbf{q}}^-$  is the set of negative keys of the given query  $\mathbf{q}$ , which is introduced in Sec. 3.3.  $\mathcal{L}_{\text{MSE}}(\mathbf{q}, \mathbf{k}^+) = \|\mathbf{q} - \mathbf{k}^+\|_2^2$ , which maximizes the similarity of positive pairs  $(\mathbf{q}, \mathbf{k}^+)$  directly.

The pulling objective is *weighted* over each positive pair

$$\mathcal{L}_{\text{pull}} = \frac{1}{C} \sum_{c=0}^{C-1} w_c^* \sum_{(\mathbf{q}, \mathbf{k}^+) \in \mathcal{K}_c^+} \mathcal{L}_{\text{pull}}(\mathbf{q}, \mathbf{k}^+), \quad (5)$$

where  $\mathcal{K}_c^+$  indicates the set of positive keys for category  $c$  described later in Sec. 3.3.  $w_c^*$  is the weight of class  $c$ , which is dynamically adjusted and discussed in Sec. 3.5.  $\mathcal{L}_{\text{pull}}(\mathbf{q}, \mathbf{k}^+)$  is the pulling loss given a pair of positive features, which is either MSE or InfoNCE (Oord et al., 2018).

### 3.2 Preliminary: Fourier Domain Adaptation

Fig. 4 illustrates how Fourier domain adaptation (FDA) (Yang and Soatto, 2020) works. In summary, given a source image  $\mathbf{x}^s$  and a target image  $\mathbf{x}^t$ , FDA transfers the source sample into target style, i.e.,  $\mathcal{T}(\mathbf{x}^s)$ , where  $\mathcal{T}(\cdot)$  indicates the transformation function, e.g., FDA (Yang and Soatto, 2020). Specifically, for every single channel image  $\mathbf{x} \in \mathbb{R}^{H \times W}$ :

$$\mathcal{F}(\mathbf{x})(m, n) = \sum_{h, w} \mathbf{x}(h, w) \exp \left[ -j2\pi \left( \frac{h}{H}m + \frac{w}{W}n \right) \right], \quad (6)$$

where  $\mathcal{F}$  is the Fourier transform function of an RGB image, and  $j^2 = -1$ . It can be efficiently implemented by the FFT algorithm (Frigo and Johnson, 1998). Accordingly,  $\mathcal{F}^{-1}$  is the inverse function, mapping spectral signals back to RGB image spaces. Next, (Yang and Soatto, 2020) define a binary mask  $\mathbf{M}_\beta \in \{0, 1\}^{H \times W}$ , whose value keeps zero except for the center region, according to a specific control value of  $\beta \in (0, 1)$ . Concretely, when we assume the center of the image is  $(0, 0)$ , the formulation becomes:

$$\mathbf{M}_\beta(h, w) = \mathbb{1}_{(h, w) \in [-\beta H : \beta H, -\beta W : \beta W]}, \quad (7)$$

where  $\mathbb{I}[\cdot]$  is the binary indicator.

Given a source image  $\mathbf{x}^s$  and a target image  $\mathbf{x}^t$ , FDA transfers the source sample into target style by:

$$\mathcal{T}(\mathbf{x}^s) = \mathcal{F}^{-1}[\mathbf{M}_\beta \odot \mathcal{F}^A(\mathbf{x}^t) + (1 - \mathbf{M}_\beta) \odot \mathcal{F}^A(\mathbf{x}^s), \mathcal{F}^P(\mathbf{x}^s)], \quad (8)$$

where  $\mathcal{F}^A, \mathcal{F}^P : \mathbb{R}^{H \times W \times 3} \rightarrow \mathbb{R}^{H \times W \times 3}$  be the amplitude and phase components of the Fourier transform  $\mathcal{F}$  of an RGB image, respectively, and “ $\odot$ ” is the element-wise dot production. The underlying assumption is that the *low-frequency* part of the amplitude contains domain-specific information. Therefore, replacing the low-frequency part of  $\mathcal{F}^A(\mathbf{x}^s)$  by that of the target image  $\mathbf{x}^t$  is all we need to obtain  $\mathcal{T}(\mathbf{x}^s)$ . Based on these operations, those pseudo-target images  $\mathcal{T}(\mathbf{x}^s)$  should:

- *Guarantee semantic alignment at the pixel-level with  $\mathbf{x}^s$* , which means for each pixel  $(h, w)$ , the ground-truth label of  $\mathcal{T}(\mathbf{x}^s)(h, w)$  keeps the same with that of  $\mathbf{x}^s(h, w)$ . This is because the low-level spectrum (amplitude) can vary significantly *without* affecting the perception of high-level semantics as demonstrated by (Yang and Soatto, 2020).
- *Appear in the style of target image  $\mathbf{x}^t$* . This is because the low-level spectrum (amplitude) controls the appearance of an image according to (Yang and Soatto, 2020).

These two characteristics together make it possible to assign precise positive samples  $(\mathbf{q}, \mathbf{k}^+)$ , allowing T2S-DA to learn similar cross-domain features regarding each category.

### 3.3 Pulling Target to Source

In this section, we describe how to generate positive pairs that *exactly* belong to the same category without target annotations. Next, we take  $\mathcal{L}_{\text{InfoNCE}}$  as the alignment objective, and provide detailed formulations.

We employ an image translation engine to make sure cross-domain positive pairs belong to the same category. Illustrated in Fig. 3, we first feed source data  $\mathbf{x}^s$  into the image translation engine  $\mathcal{T}$  (FDA (Yang and Soatto, 2020) in this paper) to produce *pseudo-target* data  $\mathcal{T}(\mathbf{x}^s)$ , which naturally have annotations, and then urge the model to learn similar features across source and pseudo-target domains regarding each category, *i.e.*, pulling features of  $\mathcal{T}(\mathbf{x}^s)$  close to features of  $\mathbf{x}^s$  for each class. Formulations are provided as follows.

**Queries  $\mathbf{q}$**  are features to be optimized, and thus they come from pseudo-target images  $\mathcal{T}(\mathbf{x}^s)$

$$\mathcal{Q}_c = \{g_s(h_s(\mathcal{T}(\mathbf{x}^s)))(j) \mid y^s(j, c) = 1\}, \quad (9)$$

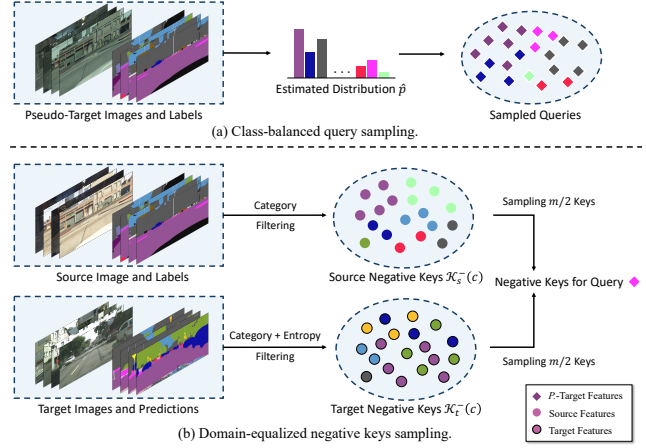


**Fig. 5 Illustration of our sampling strategies** introduced in Sec 3.4. (a) Class-balanced query sampling means we first estimate the current label distribution and then sample queries that follow the estimated distribution. (b) Domain-equalized negative keys sampling indicates we equally sample  $m/2$  negative keys for each query from source and target, respectively.

where  $j = 1, 2, \dots, h \times w$  is the pixel index, and we randomly sample  $n_q(c)$  queries for class  $c$  at each iteration, which will be discussed later in Sec. 3.4.

**Positive pairs  $(\mathbf{q}, \mathbf{k}^+)$**  are the crux for T2S-DA. To learn similar cross-domain features, their agreements are supposed to be maximized. Given a query  $\mathbf{q} \in \mathcal{Q}_c$  belongs to class  $c$ , its positive key  $\mathbf{k}^+$  is defined as the *source prototype* of class  $c$  generated by the momentum teacher. Concretely, given a mini-batch  $\mathcal{B} = (\mathbf{x}^s, \mathbf{y}^s, \mathbf{x}^t)$ , we compute the source prototype of class  $c$  by

$$\mathbf{k}_c^+ = \frac{\sum_{j=1}^{h \times w} \mathbb{I}[y^s(j, c) = 1] \cdot [g_t(h_t(\mathbf{x}^s))](j)}{\sum_{j=1}^{h \times w} \mathbb{I}[y^s(j, c) = 1]}. \quad (10)$$

Therefore, the set of positive pairs is defined as

$$\mathcal{K}^+ = \bigcup_{c=0}^{C-1} \{(\text{norm}(\mathbf{q}), \text{norm}(\mathbf{k}_c^+)) \mid \mathbf{q} \in \mathcal{Q}_c\}, \quad (11)$$

where  $\text{norm}(\cdot)$  represents the  $\ell_2$ -norm, and  $\mathcal{Q}_c$  is the set of candidate queries defined in Eq. (9). Thanks to the image translation engine, we manage to conduct  $\mathbf{q}$  and  $\mathbf{k}^+$  that belong to the *exact* category even without target labels.

**Negative pairs  $(\mathbf{q}, \mathbf{k}^-)$**  are used to avoid model collapse (He et al., 2020; Chen et al., 2020) in InfoNCE (Oord et al., 2018), which is not out main focus. Given a query  $\mathbf{q} \in \mathcal{Q}_c$  belongs to class  $c$ , its negative keys consist of features from both domains. For source features, we simply choose features that do not belong to category  $c$

$$\mathcal{K}_s^-(c) = \{g_t(h_t(\mathbf{x}^s)))(j) \mid y^s(j, c) = 0\}, \quad (12)$$

where  $j = 1, 2, \dots, h \times w$  denotes the pixel index. The subscript  $s$  here stands for “source”. For target features, inspired by (Wang et al., 2022) and (Wang et al., 2023d), we take

those unreliable features into consideration, fully mining the inherited information behind the target domain. Specifically, we regard features (1) whose confidence is in the last  $\alpha$  percent and (2) are predicted not to belong to category  $c$  as candidate negative samples

$$\mathcal{K}_t^-(c) = \{g_t(h_t(\mathbf{x}^t))(j) \mid \max_{c'} f_t(h_t(\mathbf{x}^t))(j, c') < \gamma, \hat{y}^t(j, c) = 0\}, \quad (13)$$

where  $\max_{c'} f_t(h_t(\mathbf{x}^t))(j, c')$  indicates the confidence (*i.e.*, maximum probability) of target image  $\mathbf{x}^t$  at pixel  $j$ . The subscript  $t$  here stands for “target”.  $\gamma$  is the confidence threshold related to unreliable partition  $\alpha$ , satisfying

$$\sum_{j=1}^{h \times w} \mathbb{1}[\max_{c'} f_t(h_t(\mathbf{x}^t))(j, c') < \gamma] = \alpha \cdot (hw), \quad (14)$$

*i.e.*,  $\gamma = \text{np.percentile}(\text{C.flatten}(), 100 * \alpha)$ , and  $\text{C}$  is the confidence matrix. Overall, the set of negative keys for query  $\mathbf{q}$  is:

$$\mathcal{K}_q^- = \bigcup_{c=0}^{C-1} \{\text{norm}(\mathbf{k}_c^-) \mid \mathbf{k}_c^- \in \mathcal{K}_s^-(c) \cup \mathcal{K}_t^-(c)\}. \quad (15)$$

**Discussion.** T2S-DA tries to make target features (usually noisy) close to source features without target annotations. Therefore, we regard pseudo-target features as queries and try to make them similar to *consistent* positive keys (*i.e.*, source features extracted by the momentum teacher).

### 3.4 Sampling Strategies

**Class-balanced query sampling.** Semantic segmentation usually suffers from a long-tailed label distribution. To alleviate this issue, a vanilla method is class-equalized query sampling (CEQS), treating all categories equally, *i.e.*, the number of queries  $n_q(c)$  of class  $c$  equals to  $n$  for each  $c$ . However, CEQS tends to oversample rare classes whose features are usually noisy and unstable, leading to extra training noise. To this end, we adopt class-balanced query sampling (CBQS) based on the label distribution of the current mini-batch. Specifically, given an input mini-batch  $\mathcal{B} = (\mathbf{x}^s, \mathbf{y}^s, \mathbf{x}^t)$ , we first compute the distribution of  $\mathbf{y}^s$

$$\hat{p}(c) = \frac{\sum_{j=1}^{h \times w} \mathbb{1}[y^s(j, c) = 1]}{\sum_{c=0}^{C-1} \sum_{j=1}^{h \times w} \mathbb{1}[y^s(j, c) = 1]}. \quad (16)$$

Next, based on  $\hat{\mathbf{p}}$  and the base sample number  $n$ , we define  $n_q(c) = \lceil C \cdot \hat{p}(c) \cdot n \rceil$ .

**Domain-equalized negative pair sampling.** After we get the set of candidate negative pairs, a straightforward solution is to sample  $m$  negative pairs from  $\mathcal{K}^-$  directly. However, the proportion of negative samples from each domain

(*i.e.*, source and target domains) can be unstable under such a strategy. The more samples from  $\mathcal{K}_s^-$  are introduced, the more homogeneous for all negative pairs. By contrast, the more samples from  $\mathcal{K}_t^-$  are applied, the more unstable training procedure we have due to the *false negative* issue owing to the lack of target ground truths. Therefore, to balance the stability during training (by introducing more  $\mathbf{k}^- \in \mathcal{K}_s^-$ ) and the enrichment of negative samples (by introducing more  $\mathbf{k}^- \in \mathcal{K}_t^-$ ), we adopt domain-equalized negative pair sampling (DENPS), where we randomly sample  $m/2$  features from  $\mathcal{K}_s^-$  and  $m/2$  features from  $\mathcal{K}_t^-$ .

### 3.5 Dynamic Re-Weighting

Due to the limited labeled source data and the existing domain shift, the training tends to be biased to dominant categories (Zou et al., 2018, 2019). To address this, we propose a novel dynamic re-weighting strategy which urges the model paying more attention on underperforming classes and prevents it from being overwhelmed by well-trained samples. Concretely, for class  $c$ , we define its weight  $w_c^*$  in the pulling loss as  $w_c^* = w_c / \left( \sum_{c=0}^{C-1} w_c \right)$ , where  $w_c$  is the weight computed based on the mean confidence

$$w_c = \left[ \frac{1 - \text{conf}(c)}{\max_{c'} (1 - \text{conf}(c'))} \right]^\beta, \quad (17)$$

where  $\beta = 0.5$  is a scale factor and  $\text{conf}(c)$  denotes the mean confidence (*i.e.*, maximum probability) of class  $c$  on target in current mini-batch  $\mathcal{B} = (\mathbf{x}^s, \mathbf{y}^s, \mathbf{x}^t)$ , which can be jointly calculated by pseudo-labels  $\hat{\mathbf{y}}^t$  and teacher predictions  $f_t(h_t(\mathbf{x}^t))$

$$\text{conf}(c) = \frac{\sum_{j=1}^{H \times W} \mathbb{1}[\hat{y}^t(j, c) = 1] \cdot [\max_{c'} f_t(h_t(\mathbf{x}^t))(j, c')]}{\sum_{j=1}^{H \times W} \mathbb{1}[\hat{y}^t(j, c) = 1]}. \quad (18)$$

## 4 Experiments

**Datasets.** We use three publicly available datasets.

*Cityscapes* (Cordts et al., 2016) is a dataset of real urban scenes taken from 50 cities, which is regarded as the *target* domain. Several hundreds of thousands of frames were acquired from a moving vehicle during the span of several months, covering spring, and summer. We use finely annotated images which consist of 2,975 training images, 500 validation images, and 1,525 test images, with a resolution of  $2048 \times 1024$ . Each pixel of the image is divided into 19 categories. We adopt training images as the unlabeled target domain and operate evaluations on its validation set.

*GTA5* (Richter et al., 2016) is a composite image dataset sharing 19 classes with Cityscapes, which is considered as

**Table 2** Comparison with state-of-the-art alternatives on **GTA5**  $\rightarrow$  **Cityscapes** benchmark with ResNet-101 (He et al., 2016) and DeepLab-V2 (Chen et al., 2017). The results are averaged over 3 random seeds. The top performance is highlighted in **bold** and the second score is underlined.

Method	Road	S.walk	Build.	Wall	Fence	Pole	T.lght	Sign	Veget.	Terrain	Sky	Person	Rider	Car	Truck	Bus	Train	M.bike	Bike	mIoU
source only	70.2	14.6	71.3	24.1	15.3	25.5	32.1	13.5	82.9	25.1	78.0	56.2	33.3	76.3	26.6	29.8	12.3	28.5	18.0	38.6
AdaptSeg (Tsai et al., 2018)	86.5	36.0	79.9	23.4	23.3	23.9	35.2	14.8	83.4	33.3	75.6	58.5	27.6	73.7	32.5	35.4	3.9	30.1	28.1	41.4
CyCADA (Hoffman et al., 2018)	86.7	35.6	80.1	19.8	17.5	38.0	39.9	41.5	82.7	27.9	73.6	64.9	19.0	65.0	12.0	28.6	4.5	31.1	42.0	42.7
ADVENT (Vu et al., 2019)	89.4	33.1	81.0	26.6	26.8	27.2	33.5	24.7	83.9	36.7	78.8	58.7	30.5	84.8	38.5	44.5	1.7	31.6	32.4	45.5
CBST (Zou et al., 2018)	91.8	53.5	80.5	32.7	21.0	34.0	28.9	20.4	83.9	34.2	80.9	53.1	24.0	82.7	30.3	35.9	16.0	25.9	42.8	45.9
PCLA (Kang et al., 2020)	84.0	30.4	82.4	35.3	24.8	32.2	36.8	24.5	85.5	37.2	78.6	66.9	32.8	85.5	40.4	48.0	8.8	29.8	41.8	47.7
FADA (Wang et al., 2020a)	92.5	47.5	85.1	37.6	32.8	33.4	33.8	18.4	85.3	37.7	83.5	63.2	<u>39.7</u>	87.5	32.9	47.8	1.6	34.9	39.5	49.2
MCS (Chung et al., 2022)	92.6	54.0	85.4	35.0	26.0	32.4	41.2	29.7	85.1	40.9	85.4	62.6	34.7	85.7	35.6	50.8	2.4	31.0	34.0	49.7
CAG (Zhang et al., 2019)	90.4	51.6	83.8	34.2	27.8	38.4	25.3	48.4	85.4	38.2	78.1	58.6	34.6	84.7	21.9	42.7	<b>41.1</b>	29.3	37.2	50.2
FDA (Yang and Soatto, 2020)	92.5	53.3	82.4	26.5	27.6	36.4	40.6	38.9	82.3	39.8	78.0	62.6	34.4	84.9	34.1	53.1	16.9	27.7	46.4	50.5
PIT (Lv et al., 2020)	87.5	43.4	78.8	31.2	30.2	36.3	39.3	42.0	79.2	37.1	79.3	65.4	37.5	83.2	<u>46.0</u>	45.6	<u>25.7</u>	23.5	49.9	50.6
IAST (Mei et al., 2020)	<u>93.8</u>	57.8	85.1	39.5	26.7	26.2	43.1	34.7	84.9	32.9	88.0	62.6	29.0	87.3	39.2	49.6	23.2	34.7	39.6	51.5
DACS (Tranheden et al., 2021)	89.9	39.7	<u>87.9</u>	30.7	39.5	38.5	46.4	<u>52.8</u>	<u>88.0</u>	<u>44.0</u>	<b>88.8</b>	67.2	35.8	84.5	45.7	50.2	0.0	27.3	34.0	52.1
RCCR (Zhou et al., 2022)	93.7	<u>60.4</u>	86.5	41.1	32.0	37.3	38.7	38.6	87.2	43.0	85.5	65.4	35.1	<u>88.3</u>	41.8	51.6	0.0	38.0	52.1	53.5
ProDA (Zhang et al., 2021)	91.5	52.4	82.9	42.0	<u>35.7</u>	40.0	44.4	43.3	87.0	43.8	79.5	66.5	31.4	86.7	41.1	52.5	0.0	45.4	<u>53.8</u>	53.7
CPSL (Li et al., 2022)	91.7	52.9	83.6	<u>43.0</u>	32.3	<b>43.7</b>	<u>51.3</u>	42.8	85.4	37.6	81.1	<u>69.5</u>	30.0	88.1	44.1	<b>59.9</b>	24.9	<u>47.2</u>	48.4	<u>55.7</u>
T2S-DA (ours)	<b>96.2</b>	<b>73.4</b>	<b>88.6</b>	<b>45.1</b>	<b>37.4</b>	<u>40.7</u>	<b>54.0</b>	<b>55.5</b>	<b>88.9</b>	<b>48.6</b>	<u>88.2</u>	<b>72.2</b>	<b>45.0</b>	<b>89.6</b>	<b>53.8</b>	<u>56.2</u>	1.3	<b>53.0</b>	<b>59.6</b>	<b>60.4</b>
target only <sup>†</sup>	97.1	78.7	90.3	47.3	52.3	57.0	62.9	68.4	91.7	59.2	93.8	81.6	60.5	94.0	65.6	73.8	59.3	66.9	77.0	72.5

**Table 3** Comparison with state-of-the-art alternatives on **GTA5**  $\rightarrow$  **Cityscapes** benchmark using MiT-B5 (Xie et al., 2021) as the backbone. The results are averaged over 3 random seeds. The top performance is highlighted in **bold** font. <sup>†</sup> means we reproduce the approach. We incorporate our T2S-DA with three competitive baselines, *i.e.*, DAFormer (Hoyer et al., 2022a), HRDA (Hoyer et al., 2022b), and MIC (Hoyer et al., 2023).

Method	Road	S.walk	Build.	Wall	Fence	Pole	T.lght	Sign	Veget.	Terrain	Sky	Person	Rider	Car	Truck	Bus	Train	M.bike	Bike	mIoU
source only <sup>†</sup>	76.1	18.7	84.6	29.8	31.4	34.5	44.8	23.4	87.5	42.6	87.3	63.4	21.2	81.1	39.3	44.6	2.9	33.2	29.7	46.1
DAFormer (Hoyer et al., 2022a)	95.7	70.2	89.4	53.5	<b>48.1</b>	49.6	55.8	59.4	89.9	47.9	92.5	72.2	44.7	92.3	74.5	<b>78.2</b>	65.1	55.9	61.8	68.3
DAFormer (w/ FDA) <sup>†</sup>	95.4	68.2	89.8	52.9	45.1	51.4	60.9	51.2	90.1	48.6	<b>92.6</b>	<b>75.0</b>	45.9	93.0	72.4	74.3	62.1	<b>62.3</b>	66.3	68.8
T2S-DA (w/ DAFormer)	<b>95.9</b>	<b>71.1</b>	<b>89.9</b>	<b>54.5</b>	46.6	<b>52.4</b>	<b>61.6</b>	<b>61.0</b>	<b>90.3</b>	<b>49.8</b>	92.5	74.6	<b>46.3</b>	<b>93.2</b>	<b>75.8</b>	76.3	<b>72.4</b>	58.9	<b>66.8</b>	<b>70.0</b>
target only <sup>†</sup>	98.9	80.1	93.1	63.3	60.7	64.3	68.9	70.1	93.2	59.8	94.2	82.1	67.5	94.1	75.6	83.8	79.1	68.5	77.1	77.6
HRDA (Hoyer et al., 2022b)	96.4	74.4	<b>91.0</b>	61.6	51.5	57.1	63.9	<b>69.3</b>	<b>91.3</b>	48.4	<b>94.2</b>	<b>79.0</b>	52.9	<b>93.9</b>	<b>84.1</b>	85.7	75.9	63.9	67.5	73.8
T2S-DA (w/ HRDA)	<b>96.8</b>	<b>76.2</b>	90.8	<b>67.3</b>	<b>56.1</b>	<b>59.7</b>	<b>64.3</b>	68.9	90.7	<b>53.0</b>	92.5	78.3	<b>56.1</b>	93.7	81.8	<b>86.3</b>	<b>76.2</b>	<b>67.3</b>	<b>70.1</b>	<b>75.1</b>
MIC (Hoyer et al., 2023)	97.4	80.1	91.7	61.2	56.9	59.7	66.0	<b>71.3</b>	<b>91.7</b>	51.4	<b>94.3</b>	<b>79.8</b>	56.1	94.6	85.4	90.4	80.4	64.5	68.5	75.9
T2S-DA (w/ MIC)	<b>97.5</b>	<b>80.3</b>	<b>91.8</b>	<b>64.2</b>	<b>60.1</b>	<b>60.2</b>	<b>66.3</b>	70.9	91.5	<b>54.1</b>	93.6	79.1	<b>59.3</b>	<b>94.7</b>	<b>85.8</b>	<b>90.7</b>	<b>80.9</b>	<b>66.1</b>	<b>70.4</b>	<b>76.7</b>

the *source* domain. The pixel-level semantic segmentation ground truth for 24, 966 city scene images are extracted from the physically-based rendered computer game “Grand Theft Auto V” automatically and the labeling process was completed in only 49 hours. These synthetic images are used as source domain data for training.

*Synthia* (Ros et al., 2016) is a SYNTHetic collection of Imagery and Annotations of urban scenarios, which consists of photo-realistic frames rendered from a virtual city and comes with precise pixel-level semantic annotations, which is considered as the *source* domain. We select its subset following common practices (Chen et al., 2019a; Hoyer et al., 2022a), which has 16 common semantic annotations with Cityscapes. In total, 9, 400 images with the resolution 1280 $\times$ 760 from the Synthia dataset are used as source data.

**Training.** We first resize target images to 1024  $\times$  512 and source images from GTA5 (Richter et al., 2016) to 1280  $\times$  720. Then, we random crop source images to 1024  $\times$  512 and adopt FDA (Yang and Soatto, 2020) to build the pseudo-target domain. Finally, we randomly crop them into 512  $\times$  512 for further training. We adopt AdamW (Loshchilov and Hutter, 2019) with betas (0.9, 0.999), a learning rate of  $6 \times 10^{-5}$  for the encoder and  $6 \times 10^{-4}$  for the segmentor and the projector, a weight-decay of 0.01, linear learning rate warmup schedule with  $t_{\text{warm}} = 1.5\text{k}$ . The model is trained with a batch of two source images and two target images, for 40k iterations. In accordance with (Tranheden et al., 2021), we set  $\eta = 0.999$ . Temperature  $\tau = 0.2$ , scale factor  $\beta = 0.5$ , unreliable partition  $\alpha = 50\%$ , base number of queries  $n = 128$ , number of negative pairs per query  $m = 1024$ . All experiments are conducted on 1 Telsa A100 GPU based on

**Table 4** Comparison with state-of-the-art alternatives on **Synthia**  $\rightarrow$  **Cityscapes** benchmark with ResNet-101 (He et al., 2016) and DeepLab-V2 (Chen et al., 2017). The results are averaged over 3 random seeds. The mIoU and the mIoU\* indicate we compute mean IoU over 16 and 13 categories, respectively. The top performance is highlighted in **bold** font and the second score is *underlined*.

Method	Road	S.walk	Build.	Wall*	Fence*	Pole*	T.light	Sign	Veget.	Sky	Person	Rider	Car	Bus	M.bike	Bike	mIoU	mIoU*
source only <sup>†</sup>	55.6	23.8	74.6	9.2	0.2	24.4	6.1	12.1	74.8	79.0	55.3	19.1	39.6	23.3	13.7	25.0	33.5	38.6
AdaptSeg (Tsai et al., 2018)	79.2	37.2	78.8	-	-	-	9.9	10.5	78.2	80.5	53.5	19.6	67.0	29.5	21.6	31.3	-	45.9
ADVENT (Vu et al., 2019)	85.6	42.2	79.7	8.7	0.4	25.9	5.4	8.1	80.4	84.1	57.9	23.8	73.3	36.4	14.2	33.0	41.2	48.0
CBST (Zou et al., 2018)	68.0	29.9	76.3	10.8	1.4	33.9	22.8	29.5	77.6	78.3	60.6	28.3	81.6	23.5	18.8	39.8	42.6	48.9
CAG (Zhang et al., 2019)	84.7	40.8	81.7	7.8	0.0	35.1	13.3	22.7	84.5	77.6	64.2	27.8	80.9	19.7	22.7	48.3	44.5	51.5
PIT (Lv et al., 2020)	83.1	27.6	81.5	8.9	0.3	21.8	26.4	33.8	76.4	78.8	64.2	27.6	79.6	31.2	31.0	31.3	44.0	51.8
FDA (Yang and Soatto, 2020)	79.3	35.0	73.2	-	-	-	19.9	24.0	61.7	82.6	61.4	31.1	83.9	40.8	38.4	51.1	-	52.5
FADA (Wang et al., 2020a)	84.5	40.1	83.1	4.8	0.0	34.3	20.1	27.2	84.8	84.0	53.5	22.6	85.4	43.7	26.8	27.8	45.2	52.5
MCS (Chung et al., 2022)	<b>88.3</b>	<b>47.3</b>	80.1	-	-	-	21.6	20.2	79.6	82.1	59.0	28.2	82.0	39.2	17.3	46.7	-	53.2
PyCDA (Lian et al., 2019)	75.5	30.9	83.3	20.8	0.7	32.7	27.3	33.5	84.7	85.0	64.1	25.4	85.0	45.2	21.2	32.0	46.7	53.3
PLCA (Kang et al., 2020)	82.6	29.0	81.0	11.2	0.2	33.6	24.9	18.3	82.8	82.3	62.1	26.5	85.6	48.9	26.8	52.2	46.8	54.0
DACS (Tranheden et al., 2021)	80.6	25.1	81.9	21.5	<u>2.9</u>	37.2	22.7	24.0	83.7	<b>90.8</b>	67.6	<u>38.3</u>	82.9	38.9	28.5	47.6	48.3	54.8
RCCR (Zhou et al., 2022)	79.4	45.3	83.3	-	-	-	24.7	29.6	68.9	87.5	63.1	33.8	87.0	51.0	32.1	52.1	-	56.8
IAST (Mei et al., 2020)	81.9	41.5	83.3	17.7	<b>4.6</b>	32.3	30.9	28.8	83.4	85.0	65.5	30.8	86.5	38.2	33.1	52.7	49.8	57.0
ProDA (Zhang et al., 2021)	87.1	44.0	83.2	<b>26.9</b>	0.7	42.0	45.8	<u>34.2</u>	<u>86.7</u>	81.3	68.4	22.1	<u>87.7</u>	50.0	31.4	38.6	51.9	58.5
SAC (Araslanov and Roth, 2021)	<b>89.3</b>	<u>47.2</u>	<u>85.5</u>	<u>26.5</u>	1.3	43.0	45.5	32.0	<b>87.1</b>	<u>89.3</u>	63.6	25.4	86.9	35.6	30.4	53.0	52.6	59.3
CPSL (Li et al., 2022)	87.3	44.4	83.8	25.0	0.4	42.9	<u>47.5</u>	32.4	86.5	83.3	<u>69.6</u>	29.1	<b>89.4</b>	<u>52.1</u>	<u>42.6</u>	<u>54.1</u>	<u>54.4</u>	<u>61.7</u>
T2S-DA (ours)	81.2	38.3	<b>86.0</b>	<u>26.5</u>	1.8	<b>43.8</b>	<b>48.0</b>	<b>54.6</b>	85.2	86.6	<b>73.0</b>	<b>40.8</b>	87.5	<b>52.8</b>	<b>52.2</b>	<b>62.6</b>	<b>57.6</b>	<b>65.4</b>
target only <sup>†</sup>	97.1	78.7	90.3	47.3	52.3	57.0	62.9	68.4	91.7	93.8	81.6	60.5	94.0	73.8	66.9	77.0	74.6	79.7

**Table 5** Comparison with state-of-the-art alternatives on **Synthia**  $\rightarrow$  **Cityscapes** benchmark using DAFormer (Hoyer et al., 2022a) with MiT-B5 (Xie et al., 2021). The results are averaged over 3 random seeds. The mIoU and the mIoU\* indicate we compute mean IoU over 16 and 13 categories, respectively. The top performance is highlighted in **bold** font. <sup>†</sup> means we reproduce the approach. We incorporate our T2S-DA with three competitive baselines, including DAFormer (Hoyer et al., 2022a), HRDA (Hoyer et al., 2022b), and MIC (Hoyer et al., 2023).

Method	Road	S.walk	Build.	Wall*	Fence*	Pole*	T.light	Sign	Veget.	Sky	Person	Rider	Car	Bus	M.bike	Bike	mIoU	mIoU*
source only <sup>†</sup>	56.5	23.3	81.3	16.0	1.3	41.0	30.0	24.1	82.4	82.5	62.3	23.8	77.7	38.1	15.0	23.7	42.4	47.7
DAFormer (Hoyer et al., 2022a)	84.5	40.7	88.4	41.5	<b>6.5</b>	50.0	55.0	54.6	86.0	89.8	73.2	48.2	87.2	53.2	53.9	61.7	60.9	67.4
DAFormer (w/ FDA) <sup>†</sup>	76.9	32.6	88.2	41.1	5.2	<b>54.1</b>	<b>61.3</b>	<b>55.7</b>	87.1	90.0	<b>76.8</b>	<b>48.7</b>	87.8	55.4	<b>57.2</b>	<b>63.7</b>	61.4	67.8
T2S-DA (w/ DAFormer)	87.6	46.0	<b>88.8</b>	<b>43.7</b>	6.4	53.3	59.1	54.8	<b>87.5</b>	<b>91.1</b>	75.7	47.6	<b>88.2</b>	<b>58.0</b>	54.9	62.4	<b>62.8</b>	<b>69.4</b>
target only <sup>†</sup>	98.9	80.1	93.1	63.3	60.7	64.3	68.9	70.1	93.2	94.2	82.1	67.5	94.1	83.8	68.5	77.1	78.7	82.4
HRDA (Hoyer et al., 2022b)	85.2	47.7	<b>88.8</b>	49.5	4.8	57.2	65.7	60.9	<b>85.3</b>	92.9	<b>79.4</b>	52.8	89.0	64.7	63.9	64.9	65.8	72.4
T2S-DA (w/ HRDA)	<b>85.7</b>	<b>50.3</b>	88.5	<b>50.1</b>	<b>9.7</b>	<b>61.7</b>	<b>67.1</b>	<b>62.3</b>	84.7	<b>93.0</b>	77.9	<b>56.1</b>	<b>89.3</b>	<b>68.2</b>	<b>65.7</b>	<b>70.3</b>	<b>67.5</b>	<b>73.8</b>
MIC (Hoyer et al., 2023)	86.6	50.5	89.3	47.9	7.8	59.4	66.7	63.4	87.1	<b>94.6</b>	81.0	58.9	<b>90.1</b>	61.9	67.1	64.3	67.3	74.0
T2S-DA (w/ MIC)	<b>86.1</b>	<b>51.3</b>	<b>89.4</b>	<b>49.4</b>	<b>10.3</b>	<b>60.3</b>	<b>67.0</b>	<b>64.2</b>	<b>87.2</b>	94.1	<b>81.2</b>	<b>60.7</b>	89.7	<b>64.3</b>	<b>70.3</b>	<b>68.8</b>	<b>68.4</b>	<b>74.8</b>

PyTorch (Paszke et al., 2019) and mmsegmentation (Contributors, 2020).

**Network architecture.** Start from using the DeepLab-V2 (Chen et al., 2017) as the segmentor  $f$  with ResNet-101 (He et al., 2016) as the encoder  $h$ , we adopt DACS (Tranheden et al., 2021) with two extra strategies in (Hoyer et al., 2022a) as the baseline. To further verify the efficiency of T2S-DA on recent Transformer-based networks, we use DAFormer (Hoyer et al., 2022a) as a stronger baseline, where  $h$  is the MiT-B5 encoder (Xie et al., 2021) and  $f$  is the DAFormer decoder (Hoyer et al., 2022a). The projector  $g$  takes the feature provided by the encoder as input and consists of two Conv-BN-ReLU blocks.

#### 4.1 Comparison with Existing Alternatives

We compare our T2S-DA with a large selection of previous UDA methods. The comparison is conducted on GTA5 (Richter et al., 2016)  $\rightarrow$  Cityscapes (Zhou et al., 2017) using CNN-based models and Transformer-based models in Tab. 2 and Tab. 3, respectively. Moreover, the comparison is conducted on Synthia (Ros et al., 2016)  $\rightarrow$  Cityscapes (Zhou et al., 2017) using CNN-based models and Transformer-based models in Tab. 4 and Tab. 5, respectively.

Selected methods can be summarized into three mainstream: (1) adversarial training based methods for domain alignment, including AdaptSeg (Tsai et al., 2018), CyCADA (Hoffman et al., 2018), ADVENT (Vu et al., 2019), FADA

(Wang et al., 2020a), (2) self-training based approaches, including CBST (Zou et al., 2018), IAST (Mei et al., 2020), CAG (Zhang et al., 2019), ProDA (Zhang et al., 2021), SAC (Araslanov and Roth, 2021), CPSL (Li et al., 2022), and (3) contrastive learning-based alternatives, including PLCA (Kang et al., 2020), RCCR (Zhou et al., 2022), and MCS (Chung et al., 2022). Note that, we report the performances of ProDA (Zhang et al., 2021) and CPSL (Li et al., 2022) in Tab. 2 and Tab. 4 without knowledge distillation using self-supervised trained models for a fair comparison.

As illustrated in Tab. 2 and Tab. 4, when taking DeepLabV2 (Chen et al., 2017) as the segmentation decoder and ResNet-101 (He et al., 2016) as the backbone, our T2S-DA outperforms other competitors by a large margin, achieving mIoU of 60.4% on GTA5  $\rightarrow$  Cityscapes, and 57.6% over 16 classes and 65.4% over 13 classes on Synthia  $\rightarrow$  Cityscapes, respectively. Especially for the class “sidewalk” on GTA  $\rightarrow$  Cityscapes and the class “bike” on Synthia  $\rightarrow$  Cityscapes, T2S-DA achieves IoU scores of 73.4% and 62.6%, outperforming the second place by +13.0% and +8.5%, respectively. Moreover, significant improvements are observed when comparing our T2S-DA with other contrastive learning-based methods PLCA (Kang et al., 2020), MCS (Chung et al., 2022), and RCCR (Zhou et al., 2022).

More importantly, when equipped with an advanced Transformer (Dosovitskiy et al., 2020)-based network, T2S-DA surpasses DAFormer (Hoyer et al., 2022a) by +1.7% mIoU on GTA5  $\rightarrow$  Cityscapes, +1.9% mIoU on Synthia  $\rightarrow$  Cityscapes (16 classes), and +2.0% mIoU\* on Synthia  $\rightarrow$  Cityscapes (13 classes), as illustrated in Tab. 3 and Tab. 5, respectively. Benefiting from learning similar features across domains, T2S-DA improves the performances of class “train” by +10.3% compared to DAFormer (Hoyer et al., 2022a) on GTA5  $\rightarrow$  Cityscapes benchmark. From these four tables, we can tell that by making the model learn similar features across domains, T2S-DA outperforms state-of-the-art competitors on various benchmarks.

When incorporating with more advanced baselines, *e.g.*, HRDA (Hoyer et al., 2022b) and MIC (Hoyer et al., 2023), our T2S-DA brings significant improvements *consistently* since our method is totally orthogonal to these two methods.

**Implementation details.** We simply implement our T2S-DA on the LR branch of HRDA (Hoyer et al., 2022b) with no modification. Therefore, on the basis of HRDA, the objective becomes to  $\mathcal{L} = \mathcal{L}_{LR} + \mathcal{L}_{HR} + \lambda \mathcal{L}_{LR}^{\text{pull}}$ . We did not implement  $\mathcal{L}_{\text{pull}}$  on the HR branch because we found it requires much more computational resources and GPU memory. Similarly, we also implement our T2S-DA on the LR branch of MIC (Hoyer et al., 2023) as MIC was originally developed over HRDA.

**Table 6** Comparison with previous methods on **domain generalized semantic segmentation**. All methods are trained on GTA5 and validated on Cityscapes. † indicates our reproduced results. We implement SHADE (Zhao et al., 2022) using the network architecture of DAFormer (Hoyer et al., 2022a).

Method	Venue	Backbone	mIoU
IBN-Net (Pan et al., 2018)	ECCV’18		37.4
DRPC (Yue et al., 2019)	ICCV’19		42.5
ISW (Choi et al., 2021)	CVPR’21		37.2
FSDR (Huang et al., 2021a)	CVPR’21	ResNet-101	44.8
SAN-SAW (Peng et al., 2022)	CVPR’22		45.3
SHADE (Zhao et al., 2022)	ECCV’22		46.7
DAFormer <sup>†</sup> (Hoyer et al., 2022a)	CVPR’22		46.1
SHADE <sup>†</sup> (Zhao et al., 2022)	ECCV’22	MiT-B5	46.9
T2S-DA (w/ DAFormer)	Ours		<b>48.6</b>

## 4.2 Domain Generalized Semantic Segmentation

We further evaluate our proposed T2S-DA on domain generalized (DG) semantic segmentation, where images from the target domain are inaccessible, making it more important to extract domain-invariant feature representations. We adopt the translation model provided by (Kundu et al., 2021).

Specifically, there are five types of transformation functions by default. (1) *Domain-A*: Using FDA (Yang and Soatto, 2020) while randomly selecting the target reference from a subset of style transfer dataset (Huang and Belongie, 2017). (2) *Domain-B*: Leveraging a style transfer model (Jackson et al., 2019) via randomly sampling a style embedding from a pre-defined multivariate normal distribution. (3) *Domain-C*: Using Adaptive Instance Normalization (Huang and Belongie, 2017) layers to inject style from a given reference. The reference image is randomly sampled from the style transfer dataset (Huang and Belongie, 2017). (4) *Domain-D*: Using realistic weather augmentations proposed by (Michaelis et al., 2019). (5) *Domain-E*: Using the technique proposed by (Jung et al., 2020) to generate cartoonized versions of input images. Fig. 6 illustrates the style augmentation, where we randomly augment the same source image 3 times by leveraging the off-the-shelf augmentor. Implementation details can be found here<sup>1</sup>.

Note that we cannot apply  $\mathcal{L}_{\text{target}}$ , dynamic re-weighting, and domain-equalized negative pair sampling since we fail to get target samples in DG, and thus the overall objective becomes  $\mathcal{L}_{\text{source}} + \lambda \mathcal{L}_{\text{pull}}$ .

We take DAFormer (Hoyer et al., 2022a) trained with only source images in a fully-supervised manner as the baseline. As illustrated in Tab. 6, when comparing with other alternatives, T2S-DA manages to bring significant improvements, verifying its domain-invariant property.

<sup>1</sup> <https://github.com/Haochen-Wang409/StyleTransfer>

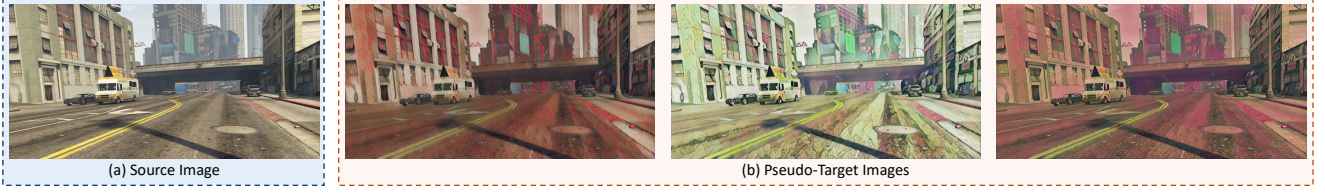


**Fig. 6** Illustration of the style augmentor proposed in (Kundu et al., 2021). We randomly augment the source image 3 times. We leverage this off-the-shelf augmentor as the image translation engine for domain generalization.

**Table 7** Ablation studies on **designs of contrastive terms**. “CE”, “q”, and “k<sup>+</sup>” are cross-entropy loss, queries, and positive keys, respectively. All experiments are conducted on the GTA5 → Cityscapes benchmark using Transformer-based models, *i.e.*, DAformer (Hoyer et al., 2022a) with MiT-B5 (Xie et al., 2021).

case	CE	q	k <sup>+</sup>	mIoU
DAFormer	source	-	-	68.3±0.5
DAFormer (w/ FDA)	p. target	-	-	68.8±0.8
vanilla contrast	source	source	source	68.5±0.3
source → target	source	source	target	68.3±1.1
source → p. target	source	source	p. target	69.0±0.3
T2S-DA (ours)	source	p. target	source	<b>70.0±0.6</b>
p. target → source	p. target	p. target	source	69.0±1.6
target → source	source	target	source	68.6±1.3

**Table 8** Ablation studies on **sampling strategies**, where “CBQS” indicates class-balanced query sampling and “DENPS” means domain-equalized negative pairs sampling. Significant improvement is observed only when combining these two techniques.

CBQS	DENPS	mIoU
		68.7±0.4
✓		68.9±0.3 ↑ 0.2
	✓	69.0±0.4 ↑ 0.3
✓	✓	<b>70.0±0.6 ↑ 1.3</b>

**Table 9** Ablation studies on **dynamic re-weighting (DRW)**. Only when applying DRW to the alignment loss  $\mathcal{L}_{\text{pull}}$  brings improvements, especially in tailed classes.

DRW	mIoU	mIoU (Tail)
none	68.9±0.6	62.0±1.1
$\mathcal{L}_{\text{target}}$	68.8±0.4 ↓ 0.1	60.1±1.3 ↓ 1.8
$\mathcal{L}_{\text{pull}}$	<b>70.0±0.6 ↑ 1.1</b>	<b>63.7±0.8 ↑ 1.7</b>

#### 4.3 Ablation Studies

In this section, we first the effectiveness of pulling target to source. Specifically, we make various permutations of where to sample (1) queries and (2) their positive keys, and where the (3) cross-entropy loss should be applied. Next, we study the effectiveness of two proposed sampling strategies and dynamic re-weighting. Then, we study the effectiveness of different objectives by replacing InfoNCE with a simple MSE to verify our motivation is *not* limited to contrastive learning. Finally, we study the effectiveness of different image translation engines and different hyper-parameters. By default, all ablations in this section are conducted on the GTA5 → Cityscapes benchmark.

**Table 10** Ablation studies on **different objectives**. When replacing the advanced InfoNCE (Zou et al., 2018) with a simple MSE, T2S-DA still brings significant improvements over baselines.

encoder	decoder	alignment	mIoU
ResNet-101	DeepLab-V2	none	56.3
ResNet-101	DeepLab-V2	MSE	58.6 ↑ 2.3
ResNet-101	DeepLab-V2	InfoNCE	<b>60.4 ↑ 4.1</b>
MiT-B5	DAFormer	none	68.3
MiT-B5	DAFormer	MSE	69.4 ↑ 1.1
MiT-B5	DAFormer	InfoNCE	<b>70.0 ↑ 1.7</b>

**Table 11** Ablations of using **different image translation models**, including FDA (Yang and Soatto, 2020), simple ColorJitter, and GaussianBlur. Also, two GAN-based methods, *i.e.*, CyCADA (Hoffman et al., 2018), and (Wang et al., 2021b) are also studied. All methods are based on DAFormer (Hoyer et al., 2022a). “Training” indicates whether the translation engine should be trained or not. “ $\mathcal{L}_{\text{pull}}$ ” means our T2S-DA objective. Without  $\mathcal{L}_{\text{pull}}$  implies that the source cross-entropy loss of DAFormer is applied on the pseudo-target domain. Significant improvements are observed consistently when we apply our  $\mathcal{L}_{\text{pull}}$  with various kinds of translation models.

Translation	Training	$\mathcal{L}_{\text{pull}}$	mIoU
-	-	-	68.3±0.5
(Yang and Soatto, 2020)	-	-	68.8±0.5
(Yang and Soatto, 2020)	-	✓	<b>70.0±0.6 ↑ 1.2</b>
ColorJitter	-	-	68.1±0.9
ColorJitter	-	✓	<b>69.0±0.6 ↑ 0.9</b>
GaussianBlur	-	-	68.4±0.7
GaussianBlur	-	✓	<b>69.5±0.5 ↑ 1.1</b>
(Hoffman et al., 2018)	✓	-	68.2±1.3
(Hoffman et al., 2018)	✓	✓	<b>69.2±0.7 ↑ 1.0</b>
(Wang et al., 2021b)	✓	-	69.3±0.6
(Wang et al., 2021b)	✓	✓	<b>70.7±0.3 ↑ 1.4</b>

**The effectiveness of pulling target to source** is studied in Tab. 7, where we take DAFormer (Hoyer et al., 2022a) as our baseline. Simply apply FDA (Yang and Soatto, 2020) to DAFormer (Hoyer et al., 2022a), *i.e.*, compute the supervised loss defined in Eq. (1) on the pseudo-target domain, brings little improvements. Vanilla contrast on the source domain also brings neglectable improvements. When simply pulling source close to target, the performance maintains 68.3% but with a larger standard deviation of 1.1%. This is because, without target labels, it is hard to conduct positive pairs precisely. To this end, we introduce an image translation engine to ensure true positive matches, but the improvements still remain limited, *i.e.*, 69.0%. However, when changing the direction of this alignment, *i.e.*, *pulling*

**Table 12** Contrastive loss weight  $\lambda$ .

$\lambda$	mIoU
0.01	68.3 $\pm$ 0.9
<b>0.1</b>	<b>70.0<math>\pm</math>0.6</b>
0.5	68.2 $\pm$ 0.6
1	67.3 $\pm$ 0.4

**Table 13** Temperature parameter  $\tau$ .

$\tau$	mIoU
0.02	69.3 $\pm$ 0.4
<b>0.2</b>	<b>70.0<math>\pm</math>0.6</b>
0.5	68.8 $\pm$ 0.7
1	69.0 $\pm$ 0.1

**Table 14** Reweighting coefficient  $\beta$ .

$\beta$	mIoU
0.1	69.9 $\pm$ 0.6
<b>0.5</b>	<b>70.0<math>\pm</math>0.6</b>
1	68.8 $\pm$ 0.4
2	69.0 $\pm$ 0.5

**Table 15** Unreliable partition  $\alpha$ .

$\alpha$	mIoU
10%	69.5 $\pm$ 0.1
<b>50%</b>	<b>70.0<math>\pm</math>0.6</b>
90%	69.4 $\pm$ 0.5

**Table 16** The number of queries  $n$  and the number of negative pairs  $m$ .

$n$	$m$	mIoU
64	1024	68.7 $\pm$ 0.3
<b>128</b>	<b>1024</b>	<b>70.0<math>\pm</math>0.6</b>
256	1024	69.3 $\pm$ 0.5
128	512	69.5 $\pm$ 0.5
128	2048	68.8 $\pm$ 0.3

target to source, however, the performance achieves 70.0%, bringing an improvement of +1.7%. In addition, if we compute cross-entropy on the pseudo target domain on the basis of T2S-DA, the performance drops to 69.0%. When simply pulling target features, the performance drops to 68.6%. The advantage of using pseudo-target features over simple target features is that the former *guarantees* the positive pairs ( $\mathbf{q}, \mathbf{k}^+$ ) belong to the *same* category, which is almost impossible when directly using target features due to the absence of target labels. In conclusion, the alignment works *only when we pull target to source leveraging the image translation engine*. An intuitive explanation is provided below. The alignment objective pulls a query  $\mathbf{q}$  to its corresponding positive key  $\mathbf{k}^+$ , which means it regards  $\mathbf{k}^+$  as an *anchor* and tries to make  $\mathbf{q}$  close to  $\mathbf{k}^+$ . Therefore, where to sample  $\mathbf{q}$  and its corresponding  $\mathbf{k}^+$  determines the effectiveness of the alignment. The selection of a pair of positive samples ( $\mathbf{q}, \mathbf{k}^+$ ) should follow these rules:

- $\mathbf{k}^+$  is expected to be categorically discriminative.
- $\mathbf{q}$  should (1) belong to a *different domain* than  $\mathbf{k}^+$ , and (2) belong to the *same category* as  $\mathbf{k}^+$ .

Therefore,

- *Sampling  $\mathbf{k}^+$  from the source domain* is the best choice because we have sufficient supervision signals on the source domain. Otherwise, when  $\mathbf{k}^+$  becomes noisy (e.g., if we let  $\mathbf{k}^+$  be target features), queries will be misled into undesirable chaos.
- As for queries  $\mathbf{q}$ , considering the two important characteristics of the introduced pseudo-target domain: (1) similar to the real target domain, and (2) naturally with pixel-wise ground truths (because the translation engine usually keeps the semantic information for each pixel), *sampling  $\mathbf{q}$  from the pseudo target domain* is the best choice.

To this end, this type of alignment works *only* when we pull target to source.

**The effectiveness of sample strategies** is studied in Tab. 8. Notably, only when combining these two strategies together brings significant improvements. On one hand, without class-balanced query sampling (CBQS), queries are easily overwhelmed by those dominant classes, e.g., “road” and “sky”. On the other hand, without domain-equalized negative pairs sampling (DENPS), the model tends to neglect target features in contrastive learning.

**The effectiveness of dynamic re-weighting (DRW)** is studied in Tab. 9. Applying DRW to  $\mathcal{L}_{\text{target}}$  rather than  $\mathcal{L}_{\text{pull}}$  can be an alternative. However, as underperforming categories tend to suffer from greater domain shifts, their target pseudo-labels can be noisy. It is risky to optimize those classes using the cross-entropy loss directly. To this end, it is better to combine DRW with  $\mathcal{L}_{\text{pull}}$ , urging the model to put more effort into learning similar cross-domain features for these categories. From the table, we can tell that *only when DRW is equipped with  $\mathcal{L}_{\text{pull}}$* , it brings significant improvements, especially in tailed classes.

**The effectiveness of different objectives** is studied in Tab. 10. InfoNCE (Zou et al., 2018) is the default alignment objective by default, however, *our motivation is not limited to contrastive learning*. Interestingly, when replacing the InfoNCE with the MSE loss between  $\ell_2$  normalized positive pairs ( $\mathbf{q}, \mathbf{k}^+$ ), it can still boost the performance with +2.3% and +1.1% mIoU improvements using CNN-based models and Transformer-based models, respectively. Details can be found in the following table.

**The effectiveness of the image translation engine** is studied in Tab. 11. Implementation details of ColorJitter and GaussianBlur are the same with SimCLR (Chen et al., 2020). We adopt FDA (Yang and Soatto, 2020) simply because it does not need extra training. This empirical evidence demonstrates that in our T2S-DA, it is not necessary to exactly *fit* the target domain. In other words, T2S-DA learns domain-invariant features *no matter what kind of transformation is adopted*. Moreover, empirical evidence illustrated in Tab. 11 indicates that the quality of the translation engine is *not* the bottleneck, but how to leverage it appropriately is, because *little* improvements are observed when applying the source cross-entropy loss on the translated pseudo-target domain.

**Ablation of  $\lambda$ .** Tab. 12 shows the performances of our T2S-DA with different weights of contrastive loss  $\lambda$ , among which  $\lambda = 0.1$  performs the best. When  $\lambda$  is too small (i.e., 0.01), the performance is close to the baseline, indicating that the target features are still undesirable, while when  $\lambda$  is too large (i.e., 1), the model tends to pay too much attention on learn similar features across domains rather than focus on the particular downstream task: semantic segmentation.

**Ablation of  $\tau$ .** Tab. 13 ablates the tunable temperature parameter  $\tau$  introduced in Eq. (2). We find that  $\tau = 0.2$  achieves

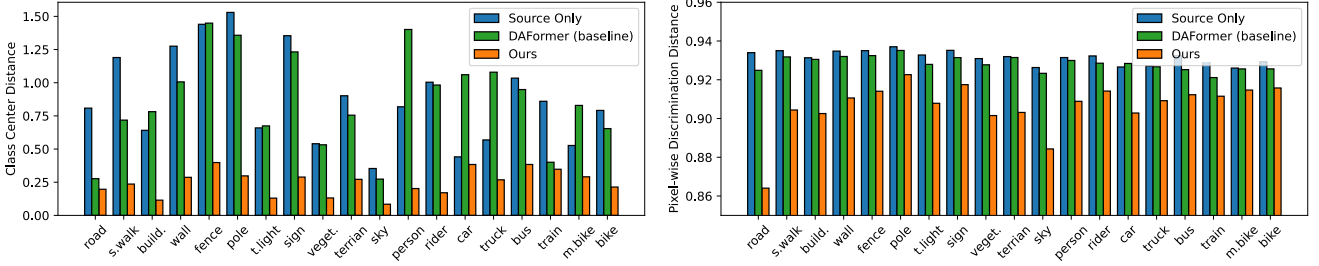


**Fig. 7 Analysis of the feature discriminativeness.** For each class, we show the values of class center distance (Wang et al., 2020a) and pixel-wise discrimination distance (Xie et al., 2023) on Cityscapes val set. For both metrics, a *smaller* value indicates *stronger* discrimination.

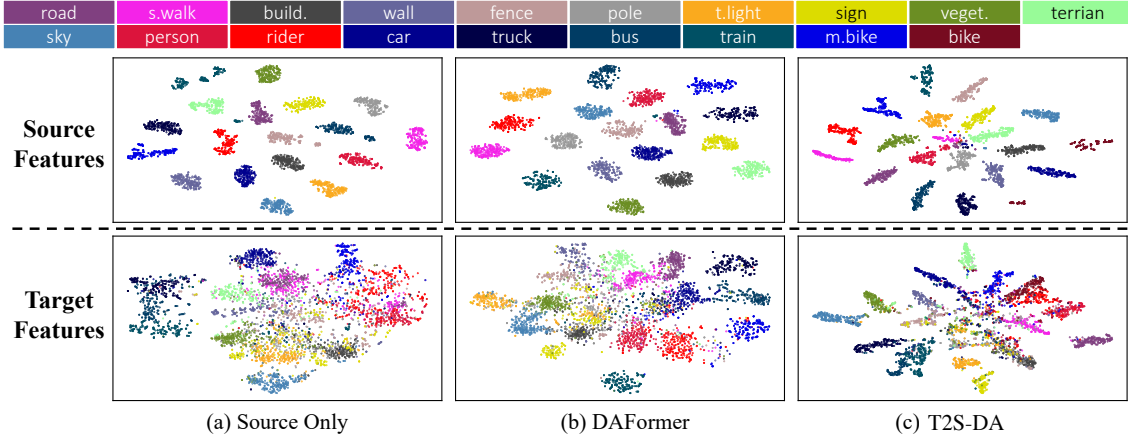


**Fig. 8 Comparison of the feature space using t-SNE (Laurens Van der Maaten, 2008) visualization between (a) the source-only baseline, (b) DAFormer (Hoyer et al., 2022a), and (c) our proposed T2S-DA.** Note that we randomly sample 256 pixels for each category for better visualization.

the best performance. One potential reason is that a smaller  $\tau$  provides less difficulty in matching the correct positive key, while a larger  $\tau$  results in too strict criteria for this dictionary look-up pretext task, which is similar to having a large contrastive loss weight  $\lambda$ .

**Ablation of  $\beta$ .** Tab. 14 studies the scale parameter of dynamic re-weighting described in Eq. (9), where  $\beta = 0.5$  yields slightly better performance, indicating that dynamic re-weighting is quite robust against  $\beta$ .

**Ablation of  $\alpha$ .** Tab. 15 ablates the unreliable partition  $\alpha$  introduced in Eq. (7), which is used to filter unreliable predictions on the target domain to be candidate negative pairs. As illustrated,  $\alpha = 50\%$  achieves slightly better performance, and our T2S-DA is insensitive to  $\alpha$ .

**Ablation of  $n$  and  $m$ .** Tab. 16 studies the base number of queries per class  $n$  and the total number of negative pairs per query  $m$  introduced in Sec. 3.3. We find that  $n = 128$  and  $m = 1024$  yield slightly better performance. Therefore, our framework is found to be stable to different  $n$  and  $m$ .

## 5 Analysis

### 5.1 Feature Discriminativeness Analysis

To verify whether our T2S-DA has indeed built a more discriminative target representation space compared with previous alternatives, we adopt metrics used in FADA (Wang et al., 2020a) and SePiCo (Xie et al., 2023) to take a closer look at what degree the representations are aligned at category-level and pixel-level, respectively. We compare the discrimination of target feature space between (1) the source-only baseline, (2) DAFormer (Hoyer et al., 2022a), and (3) our T2S-DA. We calculate these metrics on the whole Cityscapes (Cordts et al., 2016) validation set. Detailed formulations of these two metrics are given below.

**Class center distance (CCD)** is the ratio of intra-class compactness over inter-class distance (Wang et al., 2020a)

$$CDD(i) = \frac{1}{C-1} \sum_{j=0, j \neq i}^{C-1} \frac{\frac{1}{|\Omega_i|} \sum_{\mathbf{x} \in \Omega_i} \|\mathbf{x} - \boldsymbol{\mu}_i\|^2}{\|\boldsymbol{\mu}_i - \boldsymbol{\mu}_j\|^2}, \quad (19)$$

where  $\boldsymbol{\mu}_i$  is the prototype or center of category  $i$  and  $\Omega_i$  is the set of features that belong to class  $i$ .

**Pixel-wise discrimination distance (PDD)** is to evaluate the effectiveness of pixel-wise representation alignment (Xie

**Table 17** Evaluation on the **source domain** on GTA5  $\rightarrow$  Cityscapes benchmark. T2S-DA learns robust domain-invariant features with good generalization abilities since it improves the performance on *both* domains.

Method	Road	S.walk	Build.	Wall	Fence	Pole	T.light	Sign	Veget.	Terrain	Sky	Person	Rider	Car	Truck	Bus	Train	M.bike	Bike	mIoU
source only	97.6	89.7	91.8	72.4	58.9	66.2	66.6	68.1	86.1	76.1	96.6	79.8	70.0	92.7	90.8	94.4	87.5	73.7	53.9	79.6
DAFormer	97.2	87.9	91.2	68.9	55.9	65.7	67.5	71.5	85.9	74.7	96.6	79.9	75.6	92.4	89.9	93.9	92.7	80.3	64.9	80.7
T2S-DA (ours)	97.2	88.1	91.3	69.2	57.0	66.6	68.2	71.4	86.0	74.8	96.6	79.7	76.0	92.4	90.2	94.7	91.2	80.4	64.7	80.9

et al., 2023). We modify it into 1 minus its original value for a more straightforward comparison together with CCD.

$$PDD(i) = 1 - \frac{1}{|\Omega_i|} \sum_{\mathbf{x} \in \Omega_i} \frac{\cos(\mathbf{x}, \boldsymbol{\mu}_i)}{\sum_{j=0, j \neq i}^{C-1} \cos(\mathbf{x}, \boldsymbol{\mu}_j)}. \quad (20)$$

Low CCD and PDD suggest the features of the same class have been densely clustered while the distances between different categories are relatively large at category level and pixel level, respectively. We compare CCD and PDD values with source only model and DAFormer (Hoyer et al., 2022a). As illustrated in Fig. 7, T2S-DA achieves much smaller CCD and PDD values in each category compared with others. This empirical evidence verifies that by pulling target features close to source ones for each category, T2S-DA indeed learns a more discriminative target feature space, resulting in better segmentation performances.

**Visualization.** Fig. 8 gives a visualization of feature spaces of (1) the source-only baseline, (2) DAFormer (Hoyer et al., 2022a), and (3) our proposed T2S-DA, where their source features are discriminative enough but target features for source only baseline and DAFormer (Hoyer et al., 2022a) run into chaos, while our proposed T2S-DA is able to build a category-discriminative feature space. This indicates that only by self-training as DAFormer (Hoyer et al., 2022a) does, target features are not capable enough. By urging the model to learn similar cross-domain features, our proposed T2S-DA makes decision boundaries lie in low-density regions.

## 5.2 Performance on Source Domain

As our proposed T2S-DA tries to make target features as similar to source features as possible, leading to a category-discriminative feature representation space on the target domain, which implicitly assumes the model will *not* deteriorate and is able to maintain a capable feature space on the source domain during training. Therefore, we conduct experiments in Tab. 17 to verify this assumption. We do not find a significant gap between the three methods, inducing the source-only baseline, DAFormer (Hoyer et al., 2022a), and our proposed T2S-DA.

## 5.3 Qualitative Results

Fig. 9, Fig. 10, and Fig. 11 illustrate visualization results of different methods evaluated on GTA5  $\rightarrow$  Cityscapes benchmark. We compare the proposed T2S-DA with ground truths and a strong baseline DAFormer (Hoyer et al., 2022a).

From Fig. 9, we can tell that T2S-DA is able to distinguish the conjunction of “rider” and “bike/motorbike”, benefiting from pushing features for different categories away. From Fig. 10, we can tell that T2S-DA can bootstrap the performance on categories with large cross-domain feature dissimilarities (*i.e.*, “bus” in Fig. 1), indicating that T2S-DA is able to extract domain-invariant feature representations which leads to better performance. From Fig. 11, we can tell that T2S-DA pays more attention to underperforming categories, *i.e.*, “pole” and “sign” where the IoU scores of source only baseline are 34.5% and 23.4% respectively (see Tab. 1), thanks to dynamic re-weighting.

## 6 Conclusion

In this paper, we present T2S-DA, which is able to build a category-discriminative target feature space via *pulling target close to source*, leading to better segmentation results. Experimental results show significant growths, and T2S-DA proves to be very efficient at avoiding models being trapped in domain-specific styles, outperforming state-of-the-art alternatives on various UDA benchmarks. Moreover, it can be applied to DG thanks to its domain-invariant property.

**Discussion.** As discussed in (Yang and Soatto, 2020), image translation models are unstable, although it is better than using target pseudo-labels directly. Therefore, how to conduct positive pairs to alleviate the false positive issue without introducing extra noise could be further studied. Additionally, as the entire real world is the target domain in domain generalization, how to conduct a pseudo-target that is able to *almost* cover the target remains an open problem. Moreover, developing a better style transform model for UDA could be a future work, but it is quite challenging because the engine should be able to (1) generate images similar to the real target domain, and (2) guarantee semantic alignment at the pixel level. Leveraging a pre-trained fundamental generation model, *e.g.*, Stable Diffusion (Rombach et al., 2021), while

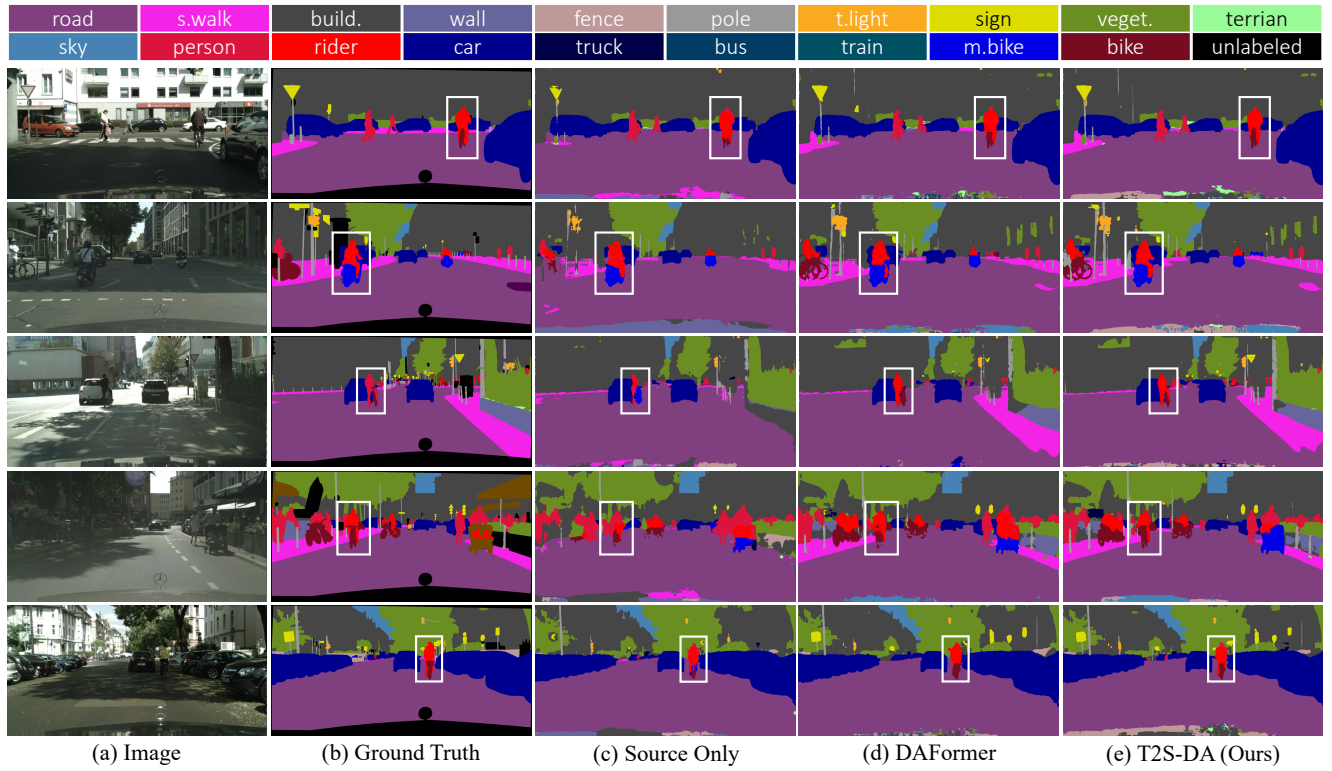


**Fig. 9** Example predictions showing better recognition and finer segmentation details of borders of “rider” and “bike/motorbike” on GTA5 → Cityscapes (best-viewed zoomed-in).

adding segmentation maps as conditions following (Zhang et al., 2023) may be a solution. However, making generative models understand semantic information and follow its guidance is still a big challenge.

## Declarations

**Acknowledgements** We would like to express our sincere gratitude to all reviewers and the Associate Editor for their valuable comments and suggestions. Their insightful feedback helped us to improve the quality of this paper significantly.

**Funding** This work was supported in part by the National Key R&D Program of China (No. 2022ZD0116500), the National Natural Science Foundation of China (No. U21B2042), and in part by the 2035 Innovation Program of CAS, and the InnoHK program.

**Data Availability** The datasets generated during and/or analyzed during the current study are available from the GTA5<sup>2</sup>, the Synthia<sup>3</sup>, and the Cityscapes<sup>4</sup>.

## References

- Araslanov, N. and Roth, S. (2021). Self-supervised augmentation consistency for adapting semantic segmentation. In *Proceedings of the IEEE/CVF Conference on Computer Vision and Pattern Recognition (CVPR)*.
- Balaji, Y., Sankaranarayanan, S., and Chellappa, R. (2018). Metareg: Towards domain generalization using meta-regularization. *Advances in Neural Information Processing Systems (NeurIPS)*.
- Ben-David, S., Blitzer, J., Crammer, K., and Pereira, F. (2006). Analysis of representations for domain adaptation. *Advances in Neural Information Processing Systems (NeurIPS)*.
- Bousmalis, K., Silberman, N., Dohan, D., Erhan, D., and Krishnan, D. (2017). Unsupervised pixel-level domain adaptation with generative adversarial networks. In *Proceedings of the IEEE/CVF Conference on Computer Vision and Pattern Recognition (CVPR)*.
- Caron, M., Touvron, H., Misra, I., Jégou, H., Mairal, J., Bojanowski, P., and Joulin, A. (2021). Emerging properties in self-supervised vision transformers. In *Proceedings of the IEEE/CVF Conference on Computer Vision and Pattern Recognition (CVPR)*.
- Chang, W.-L., Wang, H.-P., Peng, W.-H., and Chiu, W.-C. (2019). All about structure: Adapting structural information across domains for boosting semantic segmentation. In *Proceedings of the IEEE/CVF Conference on Computer Vision and Pattern Recognition (CVPR)*.
- Chen, C., Xie, W., Huang, W., Rong, Y., Ding, X., Huang, Y., Xu, T., and Huang, J. (2019a). Progressive feature alignment for unsupervised domain adaptation. In *Proceedings of the IEEE/CVF Conference on Computer Vision and Pattern Recognition (CVPR)*.
- Chen, L., Chen, H., Wei, Z., Jin, X., Tan, X., Jin, Y., and Chen, E. (2022a). Reusing the task-specific classifier as a discriminator: Discriminator-free adversarial domain adaptation. In *Proceedings of the IEEE/CVF Conference on Computer Vision and Pattern Recognition (CVPR)*.

<sup>2</sup> <https://arxiv.org/pdf/1608.02192v1.pdf>

<sup>3</sup> <https://synthia-dataset.net>

<sup>4</sup> <https://www.cityscapes-dataset.com>

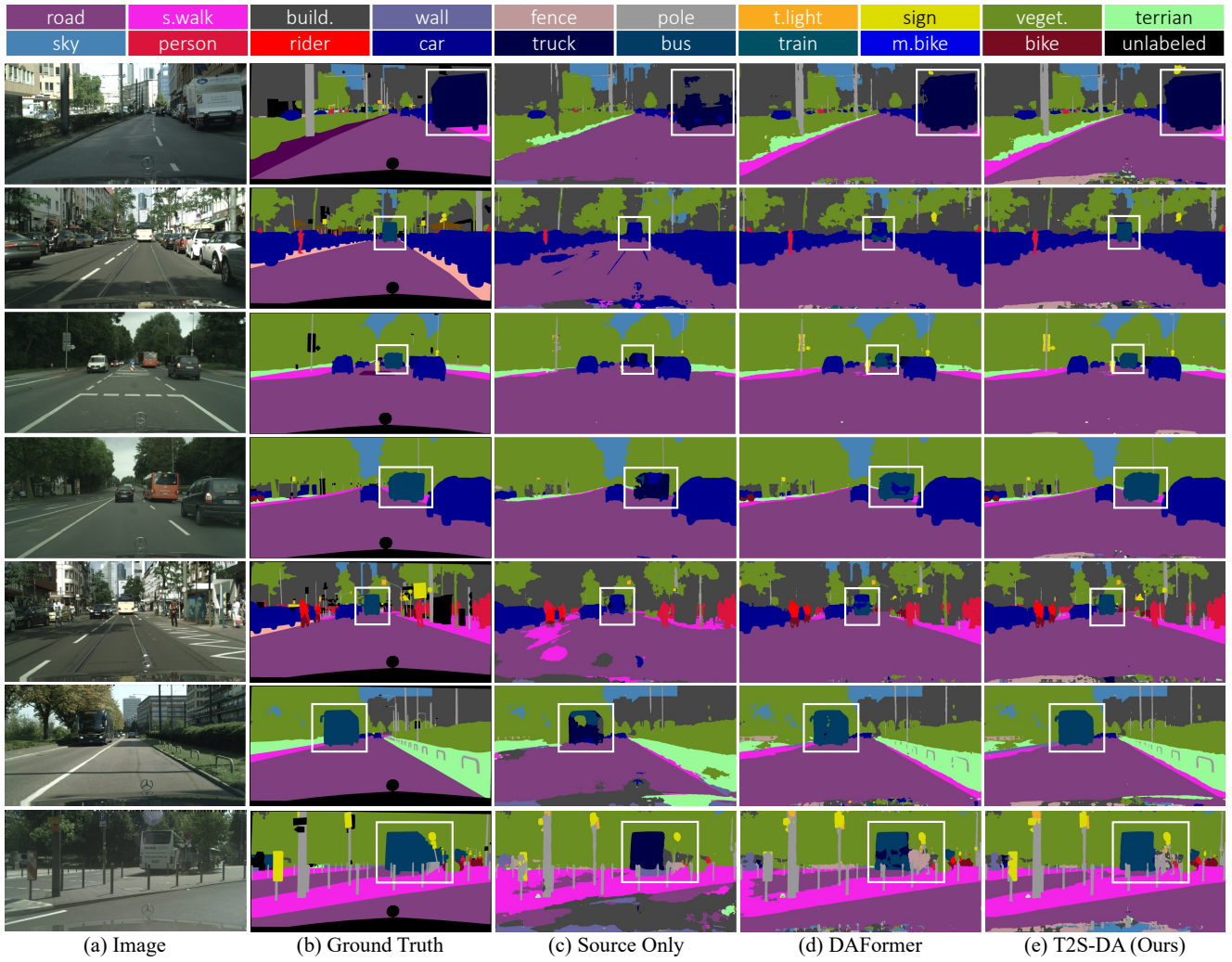


**Fig. 10** Example predictions showing a better recognition and finer segmentation details of “bus” and “truck” on GTA5 → Cityscapes, which are easily confused with a dominant category “car” (best-viewed zoomed-in).

*Recognition*, pages 7181–7190.

- Chen, L., Wei, Z., Jin, X., Chen, H., Zheng, M., Chen, K., and Jin, Y. (2022b). Deliberated domain bridging for domain adaptive semantic segmentation. *arXiv preprint arXiv:2209.07695*.
- Chen, L.-C., Papandreou, G., Kokkinos, I., Murphy, K., and Yuille, A. L. (2017). Deeplab: Semantic image segmentation with deep convolutional nets, atrous convolution, and fully connected crfs. *IEEE Transactions on Pattern Analysis and Machine Intelligence (TPAMI)*.
- Chen, T., Kornblith, S., Norouzi, M., and Hinton, G. (2020). A simple framework for contrastive learning of visual representations. In *International Conference on Machine Learning (ICML)*.
- Chen, X. and He, K. (2021). Exploring simple siamese representation learning. In *Proceedings of the IEEE/CVF Conference on Computer Vision and Pattern Recognition (CVPR)*.
- Chen, Y., Li, W., Chen, X., and Gool, L. V. (2019b). Learning semantic segmentation from synthetic data: A geometrically guided input-output adaptation approach. In *Proceedings of the IEEE/CVF Conference on Computer Vision and Pattern Recognition (CVPR)*.
- Choi, S., Jung, S., Yun, H., Kim, J. T., Kim, S., and Choo, J. (2021). Robustnet: Improving domain generalization in urban-scene segmentation via instance selective whitening. In *Proceedings of the IEEE/CVF Conference on Computer Vision and Pattern Recognition (CVPR)*.

*tion (CVPR)*.

- Chung, I., Kim, D., and Kwak, N. (2022). Maximizing cosine similarity between spatial features for unsupervised domain adaptation in semantic segmentation. In *Proceedings of the IEEE/CVF Winter Conference on Applications of Computer Vision (WACV)*.
- Contributors, M. (2020). MMSegmentation: Openmmlab semantic segmentation toolbox and benchmark. <https://github.com/open-mmlab/mms Segmentation>.
- Cordts, M., Omran, M., Ramos, S., Rehfeld, T., Enzweiler, M., Benenson, R., Franke, U., Roth, S., and Schiele, B. (2016). The cityscapes dataset for semantic urban scene understanding. In *Proceedings of the IEEE/CVF Conference on Computer Vision and Pattern Recognition (CVPR)*.
- Dosovitskiy, A., Beyer, L., Kolesnikov, A., Weissenborn, D., Zhai, X., Unterthiner, T., Dehghani, M., Minderer, M., Heigold, G., Gelly, S., et al. (2020). An image is worth 16x16 words: Transformers for image recognition at scale. In *International Conference on Learning Representations (ICLR)*.
- Dou, Q., Coelho de Castro, D., Kamnitsas, K., and Glocker, B. (2019). Domain generalization via model-agnostic learning of semantic features. *Advances in Neural Information Processing Systems (NeurIPS)*.

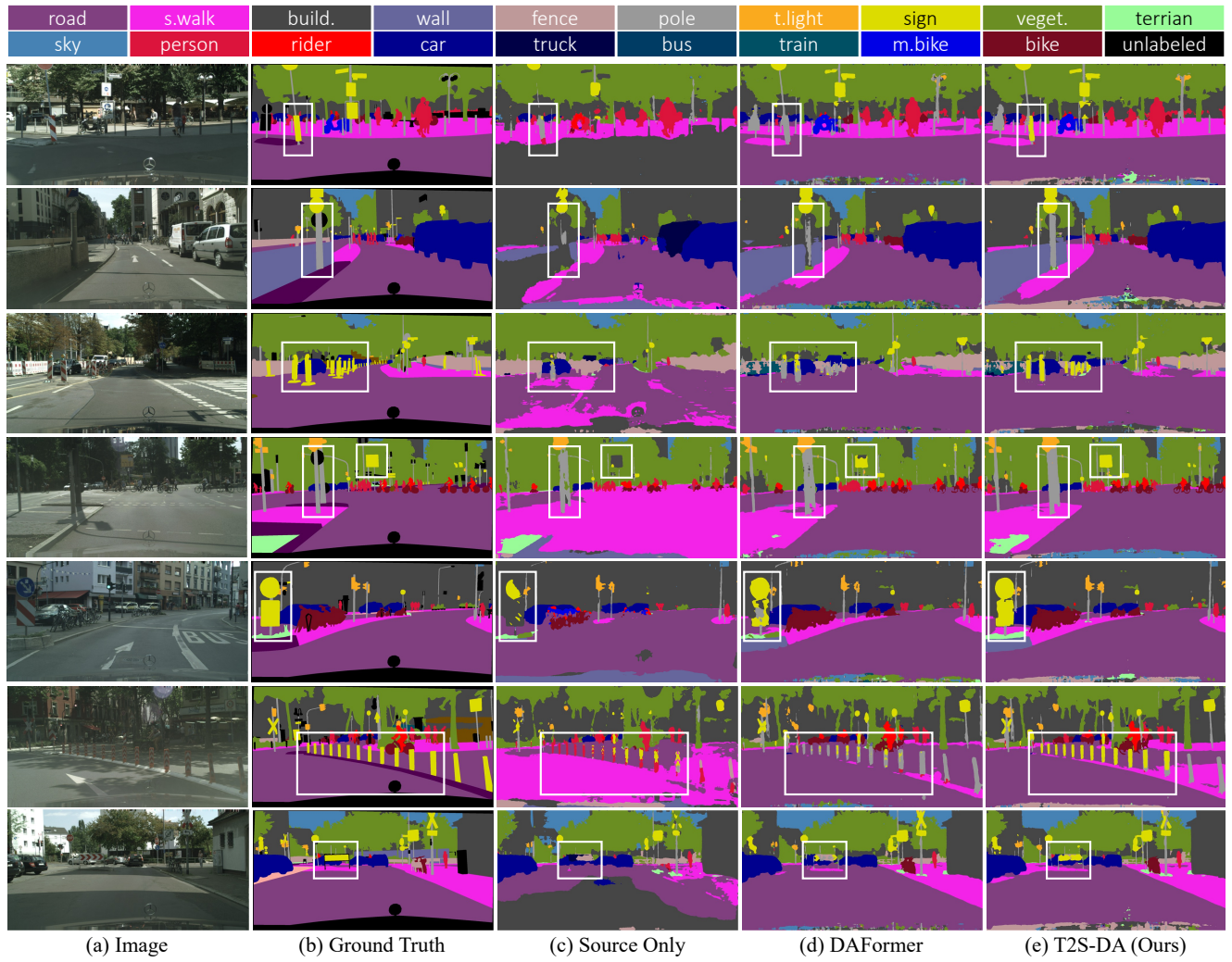


**Fig. 11** Example predictions showing better recognition and finer segmentation details of underperforming categories (“pole” and “sign”) on GTA5 → Cityscapes (best-viewed zoomed-in).

Du, Y., Fu, Z., Liu, Q., and Wang, Y. (2022a). Weakly supervised semantic segmentation by pixel-to-prototype contrast. In *Proceedings of the IEEE/CVF Conference on Computer Vision and Pattern Recognition (CVPR)*.

Du, Y., Shen, Y., Wang, H., Fei, J., Li, W., Wu, L., Zhao, R., Fu, Z., and Liu, Q. (2022b). Learning from future: A novel self-training framework for semantic segmentation. *Advances in Neural Information Processing Systems (NeurIPS)*.

Frigo, M. and Johnson, S. G. (1998). Fftw: An adaptive software architecture for the fft. In *Proceedings of the IEEE International Conference on Acoustics, Speech and Signal Processing*, volume 3, pages 1381–1384. IEEE.

Ganin, Y., Ustinova, E., Ajakan, H., Germain, P., Larochelle, H., Laviolette, F., Marchand, M., and Lempitsky, V. (2016). Domain-adversarial training of neural networks. *Journal of Machine Learning Research (JMLR)*.

Goodfellow, I., Pouget-Abadie, J., Mirza, M., Xu, B., Warde-Farley, D., Ozair, S., Courville, A., and Bengio, Y. (2014). Generative adversarial nets. *Advances in Neural Information Processing Systems (NeurIPS)*.

Gretton, A., Sejdinovic, D., Strathmann, H., Balakrishnan, S., Pontil, M., Fukumizu, K., and Sriperumbudur, B. K. (2012). Optimal kernel choice for large-scale two-sample tests. *Advances in Neural*

*Information Processing Systems (NeurIPS)*.

Grill, J.-B., Strub, F., Althé, F., Tallec, C., Richemond, P., Buchatskaya, E., Doersch, C., Avila Pires, B., Guo, Z., Gheshlaghi Azar, M., et al. (2020). Bootstrap your own latent-a new approach to self-supervised learning. *Advances in Neural Information Processing Systems (NeurIPS)*.

He, K., Fan, H., Wu, Y., Xie, S., and Girshick, R. (2020). Momentum contrast for unsupervised visual representation learning. In *Proceedings of the IEEE/CVF Conference on Computer Vision and Pattern Recognition (CVPR)*.

He, K., Zhang, X., Ren, S., and Sun, J. (2016). Deep residual learning for image recognition. In *Proceedings of the IEEE/CVF Conference on Computer Vision and Pattern Recognition (CVPR)*.

Hoffman, J., Tzeng, E., Park, T., Zhu, J.-Y., Isola, P., Saenko, K., Efros, A., and Darrell, T. (2018). Cycada: Cycle-consistent adversarial domain adaptation. In *International Conference on Machine Learning (ICML)*.

Hoffman, J., Wang, D., Yu, F., and Darrell, T. (2016). Fcns in the wild: Pixel-level adversarial and constraint-based adaptation. *arXiv preprint arXiv:1612.02649*.

Hong, W., Wang, Z., Yang, M., and Yuan, J. (2018). Conditional generative adversarial network for structured domain adaptation. In *Proceedings of the IEEE/CVF Conference on Computer Vision and*

- Pattern Recognition (CVPR)*.
- Hoyer, L., Dai, D., and Van Gool, L. (2022a). Daformer: Improving network architectures and training strategies for domain-adaptive semantic segmentation. In *Proceedings of the IEEE/CVF Conference on Computer Vision and Pattern Recognition (CVPR)*.
- Hoyer, L., Dai, D., and Van Gool, L. (2022b). Hrda: Context-aware high-resolution domain-adaptive semantic segmentation. In *European Conference on Computer Vision (ECCV)*.
- Hoyer, L., Dai, D., Wang, H., and Van Gool, L. (2023). Mic: Masked image consistency for context-enhanced domain adaptation. In *Proceedings of the IEEE/CVF Conference on Computer Vision and Pattern Recognition (CVPR)*.
- Hu, H., Cui, J., and Wang, L. (2021). Region-aware contrastive learning for semantic segmentation. In *Proceedings of the IEEE/CVF International Conference on Computer Vision (ICCV)*.
- Huang, J., Guan, D., Xiao, A., and Lu, S. (2021a). Fsrdr: Frequency space domain randomization for domain generalization. In *Proceedings of the IEEE/CVF Conference on Computer Vision and Pattern Recognition (CVPR)*.
- Huang, J., Guan, D., Xiao, A., and Lu, S. (2021b). Model adaptation: Historical contrastive learning for unsupervised domain adaptation without source data. In *Advances in Neural Information Processing Systems (NeurIPS)*.
- Huang, J., Guan, D., Xiao, A., Lu, S., and Shao, L. (2022). Category contrast for unsupervised domain adaptation in visual tasks. In *Proceedings of the IEEE/CVF Conference on Computer Vision and Pattern Recognition (CVPR)*.
- Huang, L., Zhou, Y., Zhu, F., Liu, L., and Shao, L. (2019). Iterative normalization: Beyond standardization towards efficient whitening. In *Proceedings of the IEEE/CVF Conference on Computer Vision and Pattern Recognition (CVPR)*.
- Huang, X. and Belongie, S. (2017). Arbitrary style transfer in real-time with adaptive instance normalization. In *Proceedings of the IEEE/CVF International Conference on Computer Vision (ICCV)*.
- Jackson, P. T., Abarghouei, A. A., Bonner, S., Breckon, T. P., and Obara, B. (2019). Style augmentation: data augmentation via style randomization. In *Proceedings of the IEEE/CVF Conference on Computer Vision and Pattern Recognition Workshop (CVPRW)*.
- Jung, A. B., Wada, K., Crall, J., Tanaka, S., Graving, J., Reinders, C., Yadav, S., Banerjee, J., Vecsei, G., Kraft, A., Rui, Z., Borovec, J., Vallentin, C., Zhydenko, S., Pfeiffer, K., Cook, B., Fernández, I., De Rainville, F.-M., Weng, C.-H., Ayala-Acevedo, A., Meudec, R., Laporte, M., et al. (2020). imgaug. <https://github.com/aleju/imgaug>. Online; accessed 01-Feb-2020.
- Kang, G., Wei, Y., Yang, Y., Zhuang, Y., and Hauptmann, A. (2020). Pixel-level cycle association: A new perspective for domain adaptive semantic segmentation. *Advances in Neural Information Processing Systems (NeurIPS)*.
- Kundu, J. N., Kulkarni, A., Singh, A., Jampani, V., and Babu, R. V. (2021). Generalize then adapt: Source-free domain adaptive semantic segmentation. In *Proceedings of the IEEE/CVF International Conference on Computer Vision (ICCV)*.
- Laurens Van der Maaten, G. H. (2008). Visualizing data using t-sne. *Journal of Machine Learning Research (JMLR)*.
- Lee, C.-Y., Batra, T., Baig, M. H., and Ulbricht, D. (2019). Sliced wasserstein discrepancy for unsupervised domain adaptation. In *Proceedings of the IEEE/CVF Conference on Computer Vision and Pattern Recognition (CVPR)*.
- Li, D., Yang, Y., Song, Y.-Z., and Hospedales, T. M. (2018a). Learning to generalize: Meta-learning for domain generalization. In *Proceedings of the AAAI Conference on Artificial Intelligence (AAAI)*.
- Li, D., Zhang, J., Yang, Y., Liu, C., Song, Y.-Z., and Hospedales, T. M. (2019a). Episodic training for domain generalization. In *Proceedings of the IEEE/CVF International Conference on Computer Vision (ICCV)*.
- Li, H., Pan, S. J., Wang, S., and Kot, A. C. (2018b). Domain generalization with adversarial feature learning. In *Proceedings of the IEEE/CVF Conference on Computer Vision and Pattern Recognition (CVPR)*.
- Li, R., Li, S., He, C., Zhang, Y., Jia, X., and Zhang, L. (2022). Class-balanced pixel-level self-labeling for domain adaptive semantic segmentation. In *Proceedings of the IEEE/CVF Conference on Computer Vision and Pattern Recognition (CVPR)*.
- Li, Y., Liang, F., Zhao, L., Cui, Y., Ouyang, W., Shao, J., Yu, F., and Yan, J. (2021). Supervision exists everywhere: A data efficient contrastive language-image pre-training paradigm. In *International Conference on Learning Representations (ICLR)*.
- Li, Y., Tian, X., Gong, M., Liu, Y., Liu, T., Zhang, K., and Tao, D. (2018c). Deep domain generalization via conditional invariant adversarial networks. In *European Conference on Computer Vision (ECCV)*.
- Li, Y., Yang, Y., Zhou, W., and Hospedales, T. (2019b). Feature-critic networks for heterogeneous domain generalization. In *International Conference on Machine Learning (ICML)*.
- Li, Y., Yuan, L., and Vasconcelos, N. (2019c). Bidirectional learning for domain adaptation of semantic segmentation. In *Proceedings of the IEEE/CVF Conference on Computer Vision and Pattern Recognition (CVPR)*.
- Lian, Q., Lv, F., Duan, L., and Gong, B. (2019). Constructing self-motivated pyramid curriculums for cross-domain semantic segmentation: A non-adversarial approach. In *Proceedings of the IEEE/CVF International Conference on Computer Vision (ICCV)*.
- Liu, S., Zhi, S., Johns, E., and Davison, A. J. (2022). Bootstrapping semantic segmentation with regional contrast. In *International Conference on Learning Representations (ICLR)*.
- Long, J., Shelhamer, E., and Darrell, T. (2015a). Fully convolutional networks for semantic segmentation. In *Proceedings of the IEEE/CVF Conference on Computer Vision and Pattern Recognition (CVPR)*.
- Long, M., Cao, Y., Wang, J., and Jordan, M. (2015b). Learning transferable features with deep adaptation networks. In *International Conference on Machine Learning (ICML)*.
- Long, M., Cao, Z., Wang, J., and Jordan, M. I. (2018). Conditional adversarial domain adaptation. *Advances in Neural Information Processing Systems (NeurIPS)*.
- Long, M., Zhu, H., Wang, J., and Jordan, M. I. (2016). Unsupervised domain adaptation with residual transfer networks. *Advances in Neural Information Processing Systems (NeurIPS)*.
- Loshchilov, I. and Hutter, F. (2019). Decoupled weight decay regularization. In *International Conference on Learning Representations (ICLR)*.
- Luo, Y., Liu, P., Zheng, L., Guan, T., Yu, J., and Yang, Y. (2021). Category-level adversarial adaptation for semantic segmentation using purified features. *IEEE Transactions on Pattern Analysis and Machine Intelligence (TPAMI)*.
- Luo, Y., Zheng, L., Guan, T., Yu, J., and Yang, Y. (2019). Taking a closer look at domain shift: Category-level adversaries for semantics consistent domain adaptation. In *Proceedings of the IEEE/CVF Conference on Computer Vision and Pattern Recognition (CVPR)*.
- Lv, F., Liang, T., Chen, X., and Lin, G. (2020). Cross-domain semantic segmentation via domain-invariant interactive relation transfer. In *Proceedings of the IEEE/CVF Conference on Computer Vision and Pattern Recognition (CVPR)*.
- Mei, K., Zhu, C., Zou, J., and Zhang, S. (2020). Instance adaptive self-training for unsupervised domain adaptation. In *European Conference on Computer Vision (ECCV)*.
- Michaelis, C., Mitzkus, B., Geirhos, R., Rusak, E., Bringmann, O., Ecker, A. S., Bethge, M., and Brendel, W. (2019). Benchmarking robustness in object detection: Autonomous driving when winter is coming. *arXiv preprint arXiv:1907.07484*.

- Motiian, S., Piccirilli, M., Adjero, D. A., and Doretto, G. (2017). Unified deep supervised domain adaptation and generalization. In *Proceedings of the IEEE/CVF International Conference on Computer Vision (ICCV)*.
- Murez, Z., Kolouri, S., Kriegman, D., Ramamoorthi, R., and Kim, K. (2018). Image to image translation for domain adaptation. In *Proceedings of the IEEE/CVF Conference on Computer Vision and Pattern Recognition (CVPR)*.
- Nowozin, S., Cseke, B., and Tomioka, R. (2016). f-gan: Training generative neural samplers using variational divergence minimization. *Advances in Neural Information Processing Systems (NeurIPS)*.
- Oord, A. v. d., Li, Y., and Vinyals, O. (2018). Representation learning with contrastive predictive coding. *arXiv preprint arXiv:1807.03748*.
- Pan, F., Shin, I., Rameau, F., Lee, S., and Kweon, I. S. (2020). Unsupervised intra-domain adaptation for semantic segmentation through self-supervision. In *Proceedings of the IEEE/CVF Conference on Computer Vision and Pattern Recognition (CVPR)*.
- Pan, X., Luo, P., Shi, J., and Tang, X. (2018). Two at once: Enhancing learning and generalization capacities via ibn-net. In *European Conference on Computer Vision (ECCV)*.
- Paszke, A., Gross, S., Massa, F., Lerer, A., Bradbury, J., Chanan, G., Killeen, T., Lin, Z., Gimelshein, N., Antiga, L., et al. (2019). Pytorch: An imperative style, high-performance deep learning library. *Advances in Neural Information Processing Systems (NeurIPS)*.
- Peng, D., Lei, Y., Hayat, M., Guo, Y., and Li, W. (2022). Semantic-aware domain generalized segmentation. In *Proceedings of the IEEE/CVF Conference on Computer Vision and Pattern Recognition (CVPR)*.
- Rahman, M. M., Fookes, C., Baktashmotlagh, M., and Sridharan, S. (2020). Correlation-aware adversarial domain adaptation and generalization. *Pattern Recognition*.
- Richter, S. R., Vineet, V., Roth, S., and Koltun, V. (2016). Playing for data: Ground truth from computer games. In *European Conference on Computer Vision (ECCV)*.
- Rombach, R., Blattmann, A., Lorenz, D., Esser, P., and Ommer, B. (2021). High-resolution image synthesis with latent diffusion models.
- Ronneberger, O., Fischer, P., and Brox, T. (2015). U-net: Convolutional networks for biomedical image segmentation. In *International Conference on Medical image computing and computer-assisted intervention*.
- Ros, G., Sellart, L., Materzynska, J., Vazquez, D., and Lopez, A. M. (2016). The synthia dataset: A large collection of synthetic images for semantic segmentation of urban scenes. In *Proceedings of the IEEE/CVF Conference on Computer Vision and Pattern Recognition (CVPR)*.
- Saito, K., Watanabe, K., Ushiku, Y., and Harada, T. (2018). Maximum classifier discrepancy for unsupervised domain adaptation. In *Proceedings of the IEEE/CVF Conference on Computer Vision and Pattern Recognition (CVPR)*.
- Sankaranarayanan, S., Balaji, Y., Jain, A., Lim, S. N., and Chellappa, R. (2018). Learning from synthetic data: Addressing domain shift for semantic segmentation. In *Proceedings of the IEEE/CVF Conference on Computer Vision and Pattern Recognition (CVPR)*.
- Shin, I., Woo, S., Pan, F., and Kweon, I. S. (2020). Two-phase pseudo label densification for self-training based domain adaptation. In *European Conference on Computer Vision (ECCV)*.
- Sun, B., Feng, J., and Saenko, K. (2016). Return of frustratingly easy domain adaptation. In *Proceedings of the AAAI Conference on Artificial Intelligence (AAAI)*.
- Sun, B. and Saenko, K. (2016). Deep coral: Correlation alignment for deep domain adaptation. In *European Conference on Computer Vision (ECCV)*.
- Tarvainen, A. and Valpola, H. (2017). Mean teachers are better role models: Weight-averaged consistency targets improve semi-supervised deep learning results. *Advances in Neural Information Processing Systems (NeurIPS)*.
- Tranheden, W., Olsson, V., Pinto, J., and Svensson, L. (2021). Dacs: Domain adaptation via cross-domain mixed sampling. In *Proceedings of the IEEE/CVF Winter Conference on Applications of Computer Vision (WACV)*.
- Tsai, Y.-H., Hung, W.-C., Schuster, S., Sohn, K., Yang, M.-H., and Chandraker, M. (2018). Learning to adapt structured output space for semantic segmentation. In *Proceedings of the IEEE/CVF Conference on Computer Vision and Pattern Recognition (CVPR)*.
- Tsai, Y.-H., Sohn, K., Schuster, S., and Chandraker, M. (2019). Domain adaptation for structured output via discriminative patch representations. In *Proceedings of the IEEE/CVF International Conference on Computer Vision (ICCV)*.
- Tzeng, E., Hoffman, J., Saenko, K., and Darrell, T. (2017). Adversarial discriminative domain adaptation. In *Proceedings of the IEEE/CVF Conference on Computer Vision and Pattern Recognition (CVPR)*.
- Vu, T.-H., Jain, H., Bucher, M., Cord, M., and Pérez, P. (2019). Advent: Adversarial entropy minimization for domain adaptation in semantic segmentation. In *Proceedings of the IEEE/CVF Conference on Computer Vision and Pattern Recognition (CVPR)*.
- Wang, H., Fan, J., Wang, Y., Song, K., Wang, T., Zhang, X., and Zhang, Z. (2023a). Bootstrap masked visual modeling via hard patches mining. *arXiv preprint arXiv:2312.13714*.
- Wang, H., Fan, J., Wang, Y., Song, K., Wang, T., and Zhang, Z. (2023b). Droppos: Pre-training vision transformers by reconstructing dropped positions. *Advances in Neural Information Processing Systems (NeurIPS)*.
- Wang, H., Shen, T., Zhang, W., Duan, L.-Y., and Mei, T. (2020a). Classes matter: A fine-grained adversarial approach to cross-domain semantic segmentation. In *European Conference on Computer Vision (ECCV)*.
- Wang, H., Song, K., Fan, J., Wang, Y., Xie, J., and Zhang, Z. (2023c). Hard patches mining for masked image modeling. In *Proceedings of the IEEE/CVF Conference on Computer Vision and Pattern Recognition (CVPR)*.
- Wang, H., Wang, Y., Shen, Y., Fan, J., Wang, Y., and Zhang, Z. (2023d). Using unreliable pseudo-labels for label-efficient semantic segmentation. *arXiv preprint arXiv:2306.02314*.
- Wang, H., Zheng, A., Zhao, Y., Wang, T., Zheng, G., Zhang, X., and Zhang, Z. (2024). Reconstructive visual instruction tuning. *arXiv preprint arXiv:2410.09575*.
- Wang, W., Zhou, T., Yu, F., Dai, J., Konukoglu, E., and Van Gool, L. (2021a). Exploring cross-image pixel contrast for semantic segmentation. In *Proceedings of the IEEE/CVF International Conference on Computer Vision (ICCV)*.
- Wang, Y., Fei, J., Wang, H., Li, W., Wu, L., Zhao, R., and Shen, Y. (2023e). Balancing logit variation for long-tail semantic segmentation. In *Proceedings of the IEEE/CVF Conference on Computer Vision and Pattern Recognition (CVPR)*.
- Wang, Y., Peng, J., and Zhang, Z. (2021b). Uncertainty-aware pseudo label refinery for domain adaptive semantic segmentation. In *Proceedings of the IEEE/CVF International Conference on Computer Vision (ICCV)*.
- Wang, Y., Wang, H., Shen, Y., Fei, J., Li, W., Jin, G., Wu, L., Zhao, R., and Le, X. (2022). Semi-supervised semantic segmentation using unreliable pseudo labels. In *Proceedings of the IEEE/CVF Conference on Computer Vision and Pattern Recognition (CVPR)*.
- Wang, Z., Yu, M., Wei, Y., Feris, R., Xiong, J., Hwu, W.-m., Huang, T. S., and Shi, H. (2020b). Differential treatment for stuff and things: A simple unsupervised domain adaptation method for semantic segmentation. In *Proceedings of the IEEE/CVF Conference on Computer Vision and Pattern Recognition (CVPR)*.
- Xie, B., Li, S., Li, M., Liu, C. H., Huang, G., and Wang, G. (2023). Sepico: Semantic-guided pixel contrast for domain adaptive semantic segmentation. *IEEE Transactions on Pattern Analysis and Ma-*

- chine Intelligence (TPAMI).
- Xie, E., Wang, W., Yu, Z., Anandkumar, A., Alvarez, J. M., and Luo, P. (2021). Segformer: Simple and efficient design for semantic segmentation with transformers. *Advances in Neural Information Processing Systems (NeurIPS)*.
- Yang, Y. and Soatto, S. (2020). Fda: Fourier domain adaptation for semantic segmentation. In *Proceedings of the IEEE/CVF Conference on Computer Vision and Pattern Recognition (CVPR)*.
- Yue, X., Zhang, Y., Zhao, S., Sangiovanni-Vincentelli, A., Keutzer, K., and Gong, B. (2019). Domain randomization and pyramid consistency: Simulation-to-real generalization without accessing target domain data. In *Proceedings of the IEEE/CVF International Conference on Computer Vision (ICCV)*.
- Zhang, L., Rao, A., and Agrawala, M. (2023). Adding conditional control to text-to-image diffusion models.
- Zhang, P., Zhang, B., Zhang, T., Chen, D., Wang, Y., and Wen, F. (2021). Prototypical pseudo label denoising and target structure learning for domain adaptive semantic segmentation. In *Proceedings of the IEEE/CVF Conference on Computer Vision and Pattern Recognition (CVPR)*.
- Zhang, Q., Zhang, J., Liu, W., and Tao, D. (2019). Category anchor-guided unsupervised domain adaptation for semantic segmentation. *Advances in Neural Information Processing Systems (NeurIPS)*.
- Zhao, H., Shi, J., Qi, X., Wang, X., and Jia, J. (2017). Pyramid scene parsing network. In *Proceedings of the IEEE/CVF Conference on Computer Vision and Pattern Recognition (CVPR)*.
- Zhao, Y., Zhong, Z., Zhao, N., Sebe, N., and Lee, G. H. (2022). Style-hallucinated dual consistency learning for domain generalized semantic segmentation. In *European Conference on Computer Vision (ECCV)*. Springer.
- Zheng, Z. and Yang, Y. (2021). Rectifying pseudo label learning via uncertainty estimation for domain adaptive semantic segmentation. *International Journal of Computer Vision (IJCV)*.
- Zhou, B., Zhao, H., Puig, X., Fidler, S., Barriuso, A., and Torralba, A. (2017). Scene parsing through ade20k dataset. In *Proceedings of the IEEE/CVF Conference on Computer Vision and Pattern Recognition (CVPR)*.
- Zhou, Q., Zhuang, C., Lu, X., and Ma, L. (2022). Domain adaptive semantic segmentation with regional contrastive consistency regularization. In *Proceedings of the IEEE International Conference on Multimedia and Expo (ICME)*.
- Zou, Y., Yu, Z., Kumar, B., and Wang, J. (2018). Unsupervised domain adaptation for semantic segmentation via class-balanced self-training. In *European Conference on Computer Vision (ECCV)*.
- Zou, Y., Yu, Z., Liu, X., Kumar, B., and Wang, J. (2019). Confidence regularized self-training. In *Proceedings of the IEEE/CVF Conference on Computer Vision and Pattern Recognition (CVPR)*.